JCTC Journal of Chemical Theory and Computation

Article

pubs.acs.org/JCTC

Computational Spectroscopy of Large Systems in Solution: The DFTB/PCM and TD-DFTB/PCM Approach

Vincenzo Barone,[†,‡] Ivan Carnimeo,*[,†,‡] and Giovanni Scalmani[§]

[†]Scuola Normale Superiore, Piazza dei Cavalieri 7, 56126, Pisa, Italy

[‡]INFN Sezione di Pisa, Edificio C - Polo Fibonacci Largo B. Pontecorvo, 3-56127 Pisa, Italy

[§]Gaussian, Inc., 340 Quinnipiac Street Building 40, Wallingford, Connecticut 06492, United States

ABSTRACT: The Density Functional Tight Binding (DFTB) and Time Dependent DFTB (TD-DFTB) methods have been coupled with the Polarizable Continuum Model (PCM) of solvation, aiming to study spectroscopic properties for large systems in condensed phases. The calculation of the ground and the excited state energies, together with the analytical gradient and Hessian of the ground state energy, have been implemented in a fully analytical and computationally effective approach. After sketching the theoretical background of both DFTB and PCM, we describe the details of both the formalism and the implementation. We report a number of examples ranging from vibrational to electronic spectroscopy, and we identify the strengths and the limitations of the DFTB/PCM method. We also evaluate DFTB as a component in a hybrid approach, together with a more refined quantum mechanical (QM) method and PCM, for the specific case of anharmonic vibrational spectra.

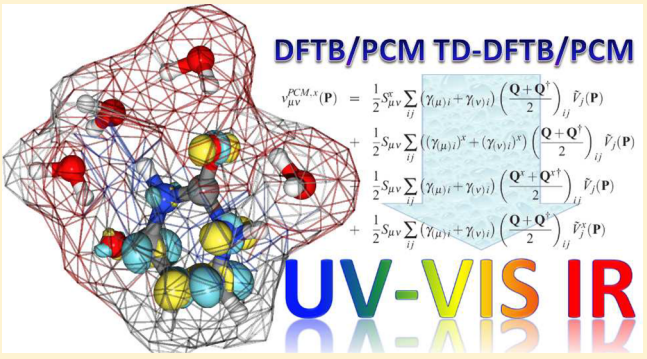

1. INTRODUCTION

Many physicochemical processes of technological and biological interest are primarily localized in a rather limited spatial region but are nevertheless significantly affected by the presence of more distant atoms, which can be broadly referred to as the "environment." Under such circumstances, focused models in which different regions are treated at different levels of sophistication become the methods of choice.[1−3] This is especially true in the case of spectroscopic processes, whose simulation requires high accuracy and the involvement of the excited states, and it is typically performed using quite costly and poorly scaling approaches.[4−7] Several integrated quantum mechanics/molecular mechanics (QM/MM) models have been introduced which proved remarkably successful and are being further complemented by continuum models to deal with bulk solvent or matrix effects.[8−11] A further degree of freedom is offered by the inclusion of an intermediate QM level employing a semiempirical method, which has the ability of describing genuine quantum effects at a reduced computational cost and with acceptable accuracy. Once again, this extension is especially significant for the study of spectroscopic processes, i.e., when the dimension of the core region is limited by the cost of the most accurate method, but the tuning effect of the microscopic environment can go beyond simple electrostatic or polarization contributions.

Self Consistent Charge Density Functional Tight Binding[12,13] (SCC-DFTB, or simply DFTB for conciseness) is an effective method for treating systems composed of a large number of atoms. Directly derived[14−16] from Density Functional Theory (DFT), it retains many characteristics of a fully QM method, and in some cases it has been found to be a valuable alternative to the other semiempirical methods based on wave function theory.[17−19] The development of a version of DFTB that employs analytical fitting of tabulated parameters (DFTBA[20]) effectively allowed DFTB to compute the molecular properties, thanks to a robust implementation of the analytical derivatives of the interaction parameters. Furthermore, the calculation of excited state energies and properties can be carried out using the time-dependent DFTB (TD-DFTB) method[21,22] which is based on the linear response theory applied to the DFTB ground state energy. In particular, our recent implementation of TD-DFTB[22] follows the formalism of Casida et al.[23] and, in contrast to a previous implementation,[21] does not require any additional parameter especially designed to describe the ground state response. In general terms, we expect the DFTB method to be very useful for the study of the spectroscopic properties of large systems, such as biological molecules or nanosized hybrid organic/inorganic aggregates.

For these reasons, the inclusion of solvation effects in the DFTB framework is of significant importance. In order to obtain accurate predictions of spectroscopic properties, the solvent effects can usually be accounted for in an implicit way. Alternatively, an explicit solvent model can be used, where e.g. a QM method is employed for the description of the solute in

Received: November 30, 2012
Published: January 31, 2013

conjunction with a less accurate and less costly method applied to the solvent molecules. An intermediate approach in which the solute and few explicit solvent molecules are embedded in a continuum polarizable solvent model has also been shown to achieve highly accurate results by including the polarization effects of the bulk of the solvent media in the most cost-effective way (see, for example, Improta and Barone[24]). Among the implicit solvent models, the Polarizable Continuum Model (PCM) in all its different variants (C-PCM,[25,26] D-PCM,[27] IEF-PCM[28−30]) is one of the most reliable methods, and it has been successfully applied for the simulation of many different properties of molecules in the condensed phase. Moreover, nonequilibrium polarization effects[31−33] can be easily accounted for, leading to a great improvement of the accuracy of the predicted spectroscopic properties.[31−33] On the other hand, the recent development of an integrated QM/MM/PCM protocol[8,9,34] allows for the treatment of solvation effects in a consistent way by including polarization effects in the MM layer. The fundamental development of the PCM solvation model is still active, and—recently—a variational formulation has been introduced for both the IEF and the conductor-like versions of the PCM,[35,36] which is likely to have a significant impact on the application of QM/MM/PCM methods to larger systems.

The accuracy of the vibrational frequencies provided by DFTB calculations is an interesting topic. Over a set of 66 organic molecules, Witek and Morokuma[18] found an overall mean absolute deviation (MAD) of 57 cm^{-1} for SCC-DFTB harmonic frequencies, with respect to fundamental frequencies from experiments. Therefore, they proposed an improved parametrization of the repulsive potential for the C−C, H−H, and C−H interactions, which reduced the MAD from 59.0 to 33.2 cm^{-1} over a set of 14 small hydrocarbon molecules.[37] Note, however, that this result was accomplished at the price of a reduced accuracy in equilibrium geometries and atomization energies. Automated parametrization procedures have been developed,[38,39] in order to fit the repulsive potentials to selected molecular data. A MAD of 33 and 38 cm^{-1} with respect to experimental fundamentals has been reported for hydrocarbon molecules[38] using two sets of parameters, developed with automated procedures. Although such approaches allowed to simulate IR[40] and Raman[41] spectra of several molecules involving only C and H atoms (hydrocarbons, fullerenes,[42] nanodiamonds,[41] nanotubes[40]), it cannot be easily translated into a general purpose protocol to improve the accuracy of predicted spectroscopic properties, mainly because the contributions from the higher derivatives of the potential are completely neglected in the computation of vibrational frequencies. A different, yet complementary, approach to vibrational spectroscopies follows a time-dependent route, employing Fourier transforms of the autocorrelation functions of dipole moments[43,44] and polarizabilities[43] accumulated during molecular dynamics simulations. In the implementation proposed by Elstner et al.,[43] large deviations were found in the position of the peaks in the Raman spectrum, such as the ones related to the O−H stretching modes of water (error of 244 cm^{-1} with respect to B3LYP/AVTZ calculations), to the C−H stretching region of glycerol (error of ∼160 cm^{-1} with respect to BLYP/AVTZ), or to the S−H stretching mode of ethanethiol (error of ∼130 cm^{-1} with respect to BLYP/AVTZ). Large errors have also been found in the position of the C−C and C−H stretchings, which have been corrected using the set of parameters developed by Witek et al.[37,38] A time-dependent approach has also been used by Spiegelman et al.[44] for the study of water−benzene complexes. In this case, the standard DFTB method has been improved with the inclusion of an empirical correction[45,46] to account for dispersion interactions, and with the use of CM3 charges[46−48] in place of Mulliken charges, to improve the treatment of the bond polarization effects on the IR intensities.

Our approach to the calculation of vibrational frequencies is based on a perturbative treatment of the molecular Hamiltonian, and it includes corrections to the harmonic frequencies involving cubic and semidiagonal quartic force constants. This method is usually referred to as VPT2,[49−51] and in our present implementation it involves the numerical evaluation of the third and fourth derivatives of the potential energy surface (PES).

In this work, we present the formalism and the implementation to include solvation effects in DFTB calculations according to the PCM model (DFTB/PCM). In section 2, the theoretical approach underlying the present implementation is described in detail for energies, first and second derivatives, including the contributions to the coupled perturbed self-consistent field (CP-SCF) and to the TD-DFTB equations. In section 3 the computational methods used in the numerical tests for the assessment of the performances of the DFTB/PCM model are briefly described. Then, the first part of section 4 consists of a general discussion about the accuracy of energies, dipoles and harmonic frequencies, along with a comparison with previously published results obtained using DFTB with other solvation models. In particular we will compare our results with the DFTB/COSMO model proposed by Elstner et al.,[52] the implementation of the Poisson−Boltzmann (DFTB/PB[53]) and the Generalized Born model (DFTB/GBSA[54]). Finally, we discuss a few significant test cases, and we propose effective protocols for the study of solvation effects on spectroscopic properties. In particular, we discuss the application of the VPT2 approach for the calculation of anharmonic frequency at the DFTB level and the use of TD-DFTB for the prediction of vertical excitation energies. In both cases, we include the effect of the solvent using the DFTB/PCM approach introduced in this work.

2. THEORY

In this section, we briefly review the formalism behind the PCM, and we discuss how the required electrostatic properties are computed using the DFTB approach. Then, we go over the expressions of the first and second derivative of the DFTB energy in solution and the PCM contribution to the TD-DFTB equations.

2.1. Brief Review of the PCM Formalism. The interaction energy between the solute charge density $n(\vec{r})$ (both nuclear and electronic) and the apparent solvent charge distribution $\sigma(\vec{s})$ is

$$E_{\text{int}} = \int_{\Gamma} \mathrm{d}\vec{s} \int \mathrm{d}\vec{r}\, \frac{n(\vec{r})\,\sigma(\vec{s})}{|\vec{r}-\vec{s}|} = \int_{\Gamma} \mathrm{d}\vec{s}\; V(\vec{s})\,\sigma(\vec{s}) \qquad (1)$$

where $\vec{r} \in \mathbb{R}^3$ and $\vec{s}$ is a point on the surface Γ that corresponds to the solute−solvent interface which separates the solute from the polarizable medium that represents the solvent. $V(\vec{s})$ is the molecular electrostatic potential generated by the charge distribution $n(\vec{r})$ at $\vec{s}$. Following the formalism of Barone et al.,[55] the free energy of the interacting solute−solvent system is

dx.doi.org/10.1021/ct301050x | J. Chem. Theory Comput. 2013, 9, 2052−2071

$$\mathcal{G} = E^0[n] + V_{NN} + \frac{1}{2}E_{\text{int}} \tag{2}$$

where $E^0[n]$ is the solute's electronic energy functional and V_{NN} is the *nuclear* electrostatic interaction, which does not depend on the electronic density. The functional forms of $E^0[n]$ and V_{NN} depend on the specific methodology employed for the calculation of the solute energy and charge density. In DFT calculations, the charge density can be expressed in a basis set of atomic orbitals (AO) as

$$n(\vec{r}) = \sum_{\mu\nu}^{N_B} P_{\mu\nu}\chi_\mu(\vec{r})\,\chi_\nu(\vec{r}) - \sum_{A}^{N_A} Z_A\delta(\vec{r} - \vec{R}_A) \tag{3}$$

where μ and ν indexes run over the functions of the AO basis set $\{\chi_\mu\}$, $\mu = 1...N_B$, and N_A is the number of atoms. If the nuclear charge density is treated as a distribution of point charges $\{Z_A\}$, the electrostatic potential at point $\vec{r}$ associated to $n(\vec{r})$ is

$$V(\vec{r}) = \sum_{\mu\nu} P_{\mu\nu}\int \mathrm{d}\vec{r}'\frac{\chi_\mu(\vec{r}')\chi_\nu(\vec{r}')}{|\vec{r} - \vec{r}'|} - \sum_A \frac{Z_A}{|\vec{r} - \vec{R}_A|} \tag{4}$$

In the practical implementation of the PCM model, the surface Γ is discretized into a certain number n_g of surface elements and the solvent charge distribution $\sigma(\vec{s})$ is expressed as a function of $\vec{r} \in \mathbb{R}^3$

$$\sigma(\vec{r}) = \sum_i^{n_g} \frac{q_i}{a_i}\phi_i(\vec{r};\,\vec{s}_i) \tag{5}$$

The quantities a_i and $\vec{s}_i$ are the geometrical parameters that define the discretization of Γ and correspond to the area and the coordinates of the center of the ith surface element. The apparent solvent charge distribution is represented by a collection of q_i point charges and $\phi_i(\vec{r};\vec{s}_i)$ Gaussian functions associated with each surface element. Having introduced such a discretization of the solute−solvent interface, the interaction energy can be written as a sum rather than an integral

$$E_{\text{int}} = \mathbf{V}^\dagger\mathbf{q} = \sum_i V_i q_i \tag{6}$$

The $\mathbf{q}$ vector contains the charges q_i, which expand $\sigma(\vec{s})$, while the elements of $\mathbf{V}$ are defined given the definition of the charge density $n(\vec{r})$ and of the $\phi_i(\vec{r};\vec{s}_i)$ functions

$$V_i = \sum_{\mu\nu} P_{\mu\nu}\langle i|\mu\nu\rangle - \sum_A Z_A\langle i|A\rangle \tag{7}$$

where

$$\begin{aligned}\langle i|A\rangle &= \int \mathrm{d}\vec{r}\int \mathrm{d}\vec{r}'\frac{\phi_i(\vec{r};\,\vec{s}_i)\delta(\vec{r}' - \vec{R}_A)}{|\vec{r} - \vec{r}'|}\\ \langle i|\mu\nu\rangle &= \int \mathrm{d}\vec{r}\int \mathrm{d}\vec{r}'\frac{\phi_i(\vec{r};\,\vec{s}_i)\chi_\mu(\vec{r}')\chi_\nu(\vec{r}')}{|\vec{r} - \vec{r}'|}\end{aligned} \tag{8}$$

At each cycle of the self-consistent field (SCF) procedure, $\mathbf{V}$ is computed from the current density matrix, and the vector of charges $\mathbf{q}$ is obtained solving the PCM equations

$$\mathbf{q} = \mathbf{QV} \tag{9}$$

The matrix $\mathbf{Q}$ actually corresponds to the inverse matrix of the PCM linear system, and it depends on the geometry of the solute, the details of the discretization of the cavity, and the particular choice of the PCM model (e.g., D-PCM,[27] C-PCM,[25,26] IEF-PCM[28−30]). The $\mathbf{Q}$ matrix is in general not symmetric, and since the energy in eq 6 actually depends quadratically on the density matrix, the polarization weights ($\mathbf{w}$)

$$\mathbf{w} = \left(\frac{\mathbf{Q} + \mathbf{Q}^\dagger}{2}\right)\mathbf{V} \tag{10}$$

and not the charges[55] are used in the PCM contribution ($v^{\text{PCM}}_{\mu\nu}$) that is added to the gas-phase Fock matrix ($F^0_{\mu\nu}$)

$$\mathbf{F} = \mathbf{F}^0 + \mathbf{v}^{\text{PCM}} \tag{11}$$

The PCM operator is defined as

$$v^{\text{PCM}}(\vec{r}) = \int_\Gamma \mathrm{d}\vec{s}\;\frac{\sigma(\vec{s})}{|\vec{r} - \vec{s}|} \tag{12}$$

and it is discretized as

$$v^{\text{PCM}}_{\mu\nu} = \sum_i w_i\langle i|\mu\nu\rangle \tag{13}$$

The interested reader can find more details in the literature about the PCM discretization,[56] the definition of different cavity models,[56,57] the practical implementation of the method,[55] and the formulation of analytical derivatives[55,56,58,59] of the solute energy including the PCM contribution.

2.2. Evaluation of Electrostatic Properties Using DFTB. In the DFTB method, the repulsive energy functional (E_{rep}) mixes together the electronic and the nuclear energy contributions (see the definition of the V_{AB} functions in Zheng et al.[13] or the derivation in Foulkes et al.[15]), so eq 2 should be written as

$$\begin{aligned}\mathcal{G} &= E^0[n] + E_{\text{rep}} + \frac{1}{2}E_{\text{int}}\\ E_{\text{rep}} &= \sum_{A>B}(V_{AB} + Z_A\gamma_{AB}Z_B)\end{aligned} \tag{14}$$

In order to evaluate E_{int}, we recall that the DFTB method is derived from the standard DFT,[12,14−16] and it uses a minimal basis set within the frozen core approximation. Therefore, the charge density of a molecule can be written as in eq 3, where the AO basis functions χ_μ are those of the minimal valence basis set and the Z_A are the nuclear valence charges. Within the DFTB approach, the atomic basis functions $\{\chi_\mu\}$ are used only as a formal tool for the evaluation of the atomic charges, so that a parametrization scheme is required for the evaluation of the integrals $\langle i|\mu\nu\rangle$, between the solute atomic charges and the basis functions of the apparent solvent charge. However, we want to avoid the introduction of new empirical parameters specifically developed for the integrals required by the PCM model. In fact, such a parametrization effort would be time-consuming, and its success could be limited if any inconsistency with the existing Fock and overlap parameters arose. For these reasons, we prefer a simpler and more pragmatic approach for the treatment of the solute−solvent electrostatic interaction, which is able to provide a robust implementation of the PCM model for DFTB, without the introduction of new and specifically optimized parameters.

We start by assuming that the total charge density of a molecule can be expressed, consistently with the DFTB formalism, as the sum of atomic densities $n_A(\vec{r} - \vec{R}_A)$

$$\tilde{n}(\vec{r}) = \sum_A n_A(\vec{r} - \vec{R}_A) \tag{15}$$

Indeed, this is one of the basic ideas behind the DFTB method. It was originally proposed by Harris[14] in order to approximate the DFT calculations for weakly interacting fragments, and it was subsequently used by Foulkes et al.[15] for the formal derivation of the DFTB. The same approach was also followed by Elstner et al.[12] in order to expand the fluctuations of the total density in atomic contributions, in the derivation of the SCC-DFTB method.[12,13,16] Then, using the formalism of Elstner et al.,[12] each of the n_A densities can be expanded in terms of radial F^A_{lm} and angular Y_{lm} functions with coefficients K^A_{lm}

$$n_A(\vec{r} - \vec{R}_A) = \sum_{l,m} K^A_{lm} F^A_{lm}(|\vec{r} - \vec{R}_A|) Y_{lm}\left(\frac{\vec{r} - \vec{R}_A}{|\vec{r} - \vec{R}_A|}\right) \tag{16}$$

If we choose Y_{lm} to be the spherical harmonics and we truncate the expansion to the first term, we obtain

$$n_A(\vec{r} - \vec{R}_A) \simeq K^A_{00} F^A_{00}(|\vec{r} - \vec{R}_A|) Y_{00} \tag{17}$$

where K^A_{00} is the first charge momentum, which can be computed as the Mulliken atomic charges, while the spherical harmonic with $l = m = 0$ is just $Y_{00} = 1/(4\pi)^{1/2}$, and we choose the function $F^A_{00} = Y^{-1}_{00}\delta(\vec{r} - R_A)$ as the radial part of the atomic densities.

Introducing these approximations, the total DFTB charge density $\tilde{n}(\vec{r})$ becomes

$$n(\vec{r}) \simeq \tilde{n}(\vec{r}) = \sum_A \Delta q_A \delta(\vec{r} - \vec{R}_A) \tag{18}$$

where the quantities Δq_A for symmetric **P** and **S** matrices are given by

$$\Delta q_A = \sum_{\substack{\mu\nu \\ \mu\in A}} \frac{1}{2}(P_{\mu\nu}S_{\mu\nu} + P_{\nu\mu}S_{\nu\mu}) - Z_A \tag{19}$$

Note that eq 18 is just an approximation for the *exact* DFTB charge density of eq 3 at large distances from the sources (i.e., the positions of the nuclei), where the electronic density also appears as a collection of point charges. The corresponding approximated molecular electrostatic potential $\tilde{V}(\vec{r})$ associated to $\tilde{n}(\vec{r})$ is readily evaluated as

$$\tilde{V}(\vec{r}) = \int d\vec{r}' \frac{\tilde{n}(\vec{r}')}{|\vec{r} - \vec{r}'|} = \sum_A \frac{\Delta q_A}{|\vec{r} - \vec{R}_A|} = \sum_A \sum_{\substack{\mu\nu \\ \mu\in A}} \frac{1}{2}\frac{(P_{\mu\nu}S_{\mu\nu} + P_{\nu\mu}S_{\nu\mu})}{|\vec{r} - \vec{R}_A|} - \sum_A \frac{Z_A}{|\vec{r} - \vec{R}_A|} \tag{20}$$

The double sum over A and over $\mu \in A$ is just a sum over the complete AO basis set for the μ index. Thus, we can establish the equality

$$\sum_A \sum_{\substack{\mu\nu \\ \mu\in A}} = \sum_{\mu\nu} \tag{21}$$

provided that we recall that $\vec{R}_A$ is always referred to the atom A on which the χ_μ atomic function is located. Throughout the rest of the paper, we will indicate with (μ) the atom where χ_μ is located. Then, the approximated electrostatic potential can also be written as follows:

$$\tilde{V}(\vec{r}) = \frac{1}{2}\sum_{\mu\nu} P_{\mu\nu}S_{\mu\nu}\left(\frac{1}{|\vec{r} - \vec{R}_{(\mu)}|} + \frac{1}{|\vec{r} - \vec{R}_{(\nu)}|}\right) - \sum_A \frac{Z_A}{|\vec{r} - \vec{R}_A|} \tag{22}$$

For each pair of basis functions χ_μ and χ_ν, we can directly compare the integrals of eq 4 with their approximation in eq 22. The resulting potential will be close to the *exact* ones as long as the approximation

$$\int d\vec{r}' \frac{\chi_\mu(\vec{r}')\,\chi_\nu(\vec{r}')}{|\vec{r} - \vec{r}'|} \simeq \frac{1}{2}S_{\mu\nu}\left(\frac{1}{|\vec{r} - \vec{R}_{(\mu)}|} + \frac{1}{|\vec{r} - \vec{R}_{(\nu)}|}\right) \tag{23}$$

is acceptable. In particular, the equality between the left- and right-hand sides of the above equation holds exactly when $\vec{r} \gg \vec{r}'$ (see the Appendix). This corresponds to the well-known fact that the potential of a distribution of point charges shows the expected $\vec{r}^{-1}$ behavior when it is evaluated far from the location of the charges, while at shorter distances this approximation is no longer valid. If we use such an approximated potential to compute the PCM charges, we expect that for solute−solvent interfaces far enough from the solute (i.e., large solute cavities) it will produce the same result as the *exact* DFTB potential. Furthermore, if the approximation in eq 23 is equally valid for all the few pairs of AO minimal valence basis functions, we expect the approximated DFTB electrostatic potential to be close to that of a true DFT method within the same minimal basis. At this point, all the physics required for the description of the electrostatic solute−solvent interaction within the DFTB approach have been accounted for. In fact, without introducing any further approximation, we take the convolution of both sides of eq 23 with the $\phi_i(\vec{r};\vec{s})$ functions, and we obtain the integrals required to setup and solve the PCM electrostatic problem:

$$\langle i|\mu\nu\rangle \simeq \frac{1}{2}S_{\mu\nu}\int d\vec{r}\ \phi_i(\vec{r};\vec{s}_i)\left(\frac{1}{|\vec{r} - \vec{R}_{(\mu)}|} + \frac{1}{|\vec{r} - \vec{R}_{(\nu)}|}\right) \tag{24}$$

Note that the integrals on the right-hand side of eq 24 do not depend on the AO basis functions. They are the only kind of integrals specifically required by the combination of DFTB and PCM, and they are easily evaluated by the same integral technology involved for *ab initio* calculations.

The interaction energy between $\tilde{n}(\vec{r})$ and $\sigma(\vec{s})$ in discretized form becomes

$$\tilde{E}_{\text{int}} = \sum_{Ai} \Delta q_A \gamma_{Ai}(|\vec{R}_A - \vec{s}_i|) q_i \tag{25}$$

which is just the classical electrostatic interaction between two distributions of point charges mediated by an isotropic Coulombic potential γ_{Ai}, which contains all the details of the physics

$$\gamma_{Ai}(|\vec{R}_A - \vec{s}_i|) = \langle A|i\rangle \tag{26}$$

The notation γ_{Ai} has been chosen in analogy with the SCC-DFTB formalism, where the electrostatic Coulombic interaction between two atoms has been indicated as γ_{AB} (see

Elstner et al.[12]). It is easy to recognize that the γ_{Ai} functions are just the integrals of the right-hand side of eq 24, so that the evaluation of the DFTB potential $\tilde{V}_i$ at the solute−solvent interface can be recast as

$$\tilde{V}_i = \frac{1}{2}\sum_{\mu\nu} P_{\mu\nu}S_{\mu\nu}(\gamma_{(\mu)i} + \gamma_{(\nu)i}) - \sum_A Z_A\gamma_{Ai} \tag{27}$$

while the PCM contribution to the Fock matrix as in eq 13 becomes

$$v_{\mu\nu}^{\mathrm{PCM}}(\mathbf{P}) = \frac{1}{2}S_{\mu\nu}\sum_i (\gamma_{(\mu)i} + \gamma_{(\nu)i})w_i(\mathbf{P}) \tag{28}$$

In eq 28, we made explicit the dependence of the polarization weights on **P** through the electrostatic potential (see eq 10), while the dependence on the set of nuclear charges $\{Z_A\}$ has been left implicit. So, each element $S_{\mu\nu}$ of the overlap matrix is multiplied by the potential generated by the solvent charges at (μ) and (ν) *nuclei*, and the factor 1/2 originates from the symmetry of **P** and **S** matrices. $v_{\mu\nu}^{\mathrm{PCM}}$ is then a pure Coulombic contribution, and its form is very similar to that of the electrostatic interaction in the bielectronic term of the gas-phase Fock matrix (see Elstner et al.[12] and Zheng et al.[13])

$$G_{\mu\nu}^0 = \frac{1}{2}S_{\mu\nu}\sum_C (\gamma_{(\mu)C} + \gamma_{(\nu)C})q_C \tag{29}$$

as these two contributions to the Fock matrix, $v_{\mu\nu}^{\mathrm{PCM}}$ and $G_{\mu\nu}^0$, only differ by the definition of the gamma functions $\gamma_{(\mu)C}$ and $\gamma_{(\mu)i}$. Equations 25 and 28 are the basic ingredients for the implementation of the DFTB/PCM model.

In the last part of this section, we add some further considerations about the electrostatics of the DFTB method, independently of its combination with the PCM model. In particular, we present what we believe is a consistent way to evaluate the dipole and higher multipole moments within the DFTB scheme, without resorting to additional parametrization. The dipole moment associated with the charge density of eq 3 is

$$\vec{\mu} = \sum_{\mu\nu} P_{\mu\nu}\int \mathrm{d}\vec{r}\ \chi_\mu(\vec{r})\ \vec{r}\chi_\nu(\vec{r}) - \sum_A Z_A\vec{R}_A \tag{30}$$

which requires the evaluation of the integrals

$$\int \mathrm{d}\vec{r}\ \chi_\mu(\vec{r})\ \vec{r}\chi_\nu(\vec{r}) \tag{31}$$

which are not provided within the usual parametrization of DFTB. Therefore, we apply the previously described approach also to the calculation of the dipole moment, which can be approximated as

$$\begin{aligned}\vec{\tilde{\mu}} &= \int \mathrm{d}\vec{r}\ \vec{r}\ \tilde{n}(\vec{r})\\ &= \sum_A \Delta q_A\vec{R}_A\\ &= \sum_A \sum_{\substack{\mu\nu\\ \mu\in A}} \frac{1}{2}(P_{\mu\nu}S_{\mu\nu} + P_{\nu\mu}S_{\nu\mu}) - \sum_A Z_A\vec{R}_A\end{aligned} \tag{32}$$

obtaining the following final expression

$$\vec{\tilde{\mu}} = \frac{1}{2}\sum_{\mu\nu} P_{\mu\nu}S_{\mu\nu}(\vec{R}_{(\mu)} + \vec{R}_{(\nu)}) - \sum_A Z_A\vec{R}_A \tag{33}$$

If we compare the dipole integrals of eq 30 with the approximated ones in eq 33, we find that the approximated dipole moment will be close to the *exact* one as long as

$$\int \mathrm{d}\vec{r}\ \chi_\mu(\vec{r})\ \vec{r}\chi_\nu(\vec{r}) \simeq \frac{1}{2}S_{\mu\nu}(\vec{R}_{(\mu)} + \vec{R}_{(\nu)}) \tag{34}$$

If we evaluate these integrals approximating the atomic functions χ_μ and χ_ν with Gaussian functions (see the Appendix), we find that eq 34 is always verified, without any restriction on the domain of $\vec{r}$. This suggests that the DFTB dipole moments can be computed using eq 33 rather than eq 30, and the accuracy should be comparable to that of a DFT calculation using a valence minimal basis set. All multipole moments up to sixth order have been implemented with this approach.

As a final note, we point out that no explicit PCM contribution needs to be added to eq 33 because the dipole moment is a first order property. In other words, when the energy in eq 14 (including the PCM contribution) has been variationally minimized, the dipole moment is simply computed from the resulting density matrix and the quantities on right-hand side of eq 34.

2.3. Analytical Derivatives of the DFTB/PCM Energy.

Using the approximations and the expressions introduced in the previous section, we now describe how to compute all the other quantities related to the electrostatic potential and needed for the evaluation of DFTB/PCM energy, its analytical first and second derivatives, and its derivative as required to solve the coupled perturbed SCF equations. The theory and implementation of the analytical derivatives of the PCM energy have been already reported in the literature,[55,56,58,59] and here we will follow the formalism described by Barone et al.[55]

We already encountered the first example of derivative of the PCM energy, since the PCM contribution to the Fock matrix is the derivative of eq 25 with respect to the elements $P_{\mu\nu}$ of the density matrix. The discussion of all the relevant aspects has been reported in the previous section (see the discussion about eq 28), so we will not come back to this issue again.

In order to compute the analytical gradient of the energy of eq 25, we need to define the derivatives of the DFTB electrostatic potential ($\tilde{V}_i^x$) with respect to an external perturbation x, corresponding to the displacement of one of the nuclei. The derivative of gamma function γ_{Ai} involves two contributions: one arises from the perturbation of the atomic coordinate $\vec{R}_A$ and the other from the change in the location of the surface element $\vec{s}_i$, which ultimately depends on the position of the nuclei through the details of the discretization of the solute−solvent interface. More formally, we can write

$$(\gamma_{Ai})^x = \langle A^x|i\rangle + \frac{\partial\langle Ai|\rangle}{\partial\vec{s}_i}\cdot\frac{\partial\vec{s}_i}{\partial x} = \langle A^x|i\rangle + \langle Ai'|\rangle\cdot\frac{\partial\vec{s}_i}{\partial x} \tag{35}$$

Thus, since any contribution from the density matrix derivative $\mathbf{P}^x$ vanishes for a variationally optimized wave function, the final form of $\tilde{V}_i^x$ is

$$\begin{aligned}\tilde{V}_i^x = &\frac{1}{2}\sum_{\mu\nu} P_{\mu\nu}S_{\mu\nu}^x(\gamma_{(\mu)i} + \gamma_{(\nu)i}) + \sum_A \Delta q_A\langle A^x|i\rangle\\ &+ \sum_A \Delta q_A\langle Ai'|\rangle\cdot\frac{\partial\vec{s}_i}{\partial x}\end{aligned} \tag{36}$$

As already noted, all the integrals involved in the above equation, i.e., $\langle A^x|i\rangle$ and $\langle Ai'|\rangle$, can be obtained using standard

integral codes, while $S^x_{\mu\nu}$ can be computed from the derivatives of the analytical functions fitting the DFTB overlap parameters.

The evaluation of the density matrix derivative $\mathbf{P}^x$ becomes necessary in order to compute higher order molecular properties, such as harmonic vibrational frequencies, infrared intensities, and vertical excitation energies within the linear response approach. The PCM contribution to the kernel of the CP-SCF equations corresponds to a Fock matrix contribution of the form $v^{\mathrm{PCM}}_{\mu\nu}(\mathbf{P}^x)$ where the polarization weights are computed using the differential density matrix, i.e.

$$v^{\mathrm{PCM}}_{\mu\nu}(\mathbf{P}^x) = \frac{1}{2}S_{\mu\nu}\sum_{ij}(\gamma_{(\mu)i}+\gamma_{(\nu)i})\left(\frac{\mathbf{Q}+\mathbf{Q}^\dagger}{2}\right)_{ij}\tilde{V}_j(\mathbf{P}^x) \tag{37}$$

It is worth to note that $\tilde{V}_j(\mathbf{P}^x)$ is only the electronic component of the electrostatic potential, since the nuclear part does not depend on $\mathbf{P}^x$. When the perturbation is an external static electric field, the right-hand side of the CP-SCF equations is given by the dipole integrals, which we compute as described in eq 33 for the DFTB method. The solution of such equations leads to the static polarizability tensor. On the other hand, when we include perturbations of the solute geometry, the right-hand side of the CP-SCF equations involves the derivatives of the PCM contribution to the Fock matrix with respect to the nuclear displacements, which can be calculated from eqs 28 and 35, together with other quantities such as the geometrical derivatives of the PCM matrix $\mathbf{Q}^x$:

$$\begin{aligned} v^{\mathrm{PCM},x}_{\mu\nu}(\mathbf{P}) = {} & \frac{1}{2}S^x_{\mu\nu}\sum_{ij}(\gamma_{(\mu)i}+\gamma_{(\nu)i})\left(\frac{\mathbf{Q}+\mathbf{Q}^\dagger}{2}\right)_{ij}\tilde{V}_j(\mathbf{P}) \\ & + \frac{1}{2}S_{\mu\nu}\sum_{ij}((\gamma_{(\mu)i})^x+(\gamma_{(\nu)i})^x)\left(\frac{\mathbf{Q}+\mathbf{Q}^\dagger}{2}\right)_{ij}\tilde{V}_j(\mathbf{P}) \\ & + \frac{1}{2}S_{\mu\nu}\sum_{ij}(\gamma_{(\mu)i}+\gamma_{(\nu)i})\left(\frac{\mathbf{Q}^x+\mathbf{Q}^{x\dagger}}{2}\right)_{ij}\tilde{V}_j(\mathbf{P}) \\ & + \frac{1}{2}S_{\mu\nu}\sum_{ij}(\gamma_{(\mu)i}+\gamma_{(\nu)i})\left(\frac{\mathbf{Q}+\mathbf{Q}^\dagger}{2}\right)_{ij}\tilde{V}^x_j(\mathbf{P}) \end{aligned} \tag{38}$$

Finally, the remaining contributions to the Hessian of the energy are rather cumbersome to assemble, but the only new quantity that needs to be evaluated is the second derivative of γ_{Ai}, which corresponds to

$$\begin{aligned} (\gamma_{Ai})^{x,y} = {} & \langle A^{xy}|i\rangle + \langle A^x|i'\rangle\cdot\frac{\partial\vec{s}_i}{\partial y} + \langle A^y|i'\rangle\cdot\frac{\partial\vec{s}_i}{\partial x} \\ & + \frac{\partial\vec{s}_i}{\partial x}\cdot\langle A|i''\rangle\cdot\frac{\partial\vec{s}_i}{\partial y} + \langle A|i'\rangle\cdot\frac{\partial^2\vec{s}_i}{\partial x\partial y} \end{aligned} \tag{39}$$

As in the case of $(\gamma_{Ai})^x$, we stress that all the additional integrals involved in the expression above, namely $S^{xy}_{\mu\nu}$, $\langle A^x|i'\rangle$, and $\langle A|i''\rangle$, are typically available from standard integral codes, while $S^{xy}_{\mu\nu}$ can be obtained from the DFTB parameters.

2.4. PCM Contribution to the TD-DFTB Equations. The application of linear response theory to the DFTB ground state is equivalent to the corresponding derivation of standard TD-DFT, as reported by Casida et al.[23] Following this approach, the final form of the TD-DFTB equations is well-known

$$\begin{pmatrix}\mathbf{A} & \mathbf{B}\\ \mathbf{B} & \mathbf{A}\end{pmatrix}\begin{pmatrix}\mathbf{X}\\ \mathbf{Y}\end{pmatrix} = \Omega\begin{pmatrix}\mathbf{1} & \mathbf{0}\\ \mathbf{0} & -\mathbf{1}\end{pmatrix}\begin{pmatrix}\mathbf{X}\\ \mathbf{Y}\end{pmatrix} \tag{40}$$

The eigenvalues Ω give the values of the vertical excitation energies, while the amplitudes for the single particle excitation and de-excitation are contained in the eigenvectors $\mathbf{X}$ and $\mathbf{Y}$, respectively. The response matrices $\mathbf{A}$ and $\mathbf{B}$ are defined as

$$\begin{aligned} A_{ai\sigma,bj\sigma'} &= (\varepsilon_{a\sigma}-\varepsilon_{i\sigma})\delta_{ab}\delta_{ij}\delta_{\sigma\sigma'} + \frac{\partial F^\sigma_{ai}}{\partial P^{\sigma'}_{bj}} \\ B_{ai\sigma,bj\sigma'} &= \frac{\partial F^\sigma_{ai}}{\partial P^{\sigma'}_{jb}} \end{aligned} \tag{41}$$

where i and j are occupied orbitals, a and b are unoccupied ones, and σ is a spin label. The usual procedure for the diagonalization of eq 40 involves the contraction of the combinations $(\mathbf{A}+\mathbf{B})$ and $(\mathbf{A}-\mathbf{B})$ with the $(\mathbf{X}+\mathbf{Y})$ and $(\mathbf{X}-\mathbf{Y})$ vectors, carried out in the AO basis. When solvation effects are added to the linear response theory according to the PCM scheme,[60] the four-index quantities in the above equations are supplemented by an explicit PCM contribution

$$\frac{\partial F^\sigma_{\mu\nu}}{\partial P^{\sigma'}_{\lambda\tau}} = \mathbf{J}_{\mu\nu\lambda\tau} + \mathbf{K}^{\sigma\sigma'}_{\mu\nu\lambda\tau} + \frac{\partial v^{\mathrm{PCM}}_{\mu\nu}}{\partial P^{\sigma'}_{\lambda\tau}} \tag{42}$$

where, as pointed out by Trani et al.,[22] the contribution to the response matrices is the sum of a Coulomb-like interaction kernel ($\mathbf{J}$) and a spin-dependent exchange-like interaction kernel ($\mathbf{K}$). The PCM contribution to the response matrices does not depend on the spin label, and it is a pure Coulomb-like term, which can be written as

$$\frac{\partial v^{\mathrm{PCM}}_{\mu\nu}}{\partial P^{\sigma'}_{\lambda\tau}} = \frac{1}{4}S_{\mu\nu}S_{\lambda\tau}\sum_{ij}[\gamma_{(\mu)i}+\gamma_{(\nu)i}]\left(\frac{\mathbf{Q}+\mathbf{Q}^\dagger}{2}\right)_{ij}[\gamma_{(\lambda)j}+\gamma_{(\tau)j}] \tag{43}$$

The extension of the TD-DFTB/PCM approach to the case of nonequilibrium solvation[31−33] is straightforward. The equilibrium $\mathbf{Q}(\varepsilon)$ matrix, which depends on the static dielectric constant ε, is simply replaced by $\mathbf{Q}(\varepsilon_\infty)$, where the optical dielectric constant ε_∞ is used in place of the static one.

3. COMPUTATIONAL METHODS

In order to test the performances of the DFTB/PCM scheme, a benchmark of 18 neutral molecules and four ions has been chosen. The DFTB method in its recently developed analytical formulation[20] (which will be referred to as DFTBA hereafter) and other popular semiempirical methods (PM6[61] and AM1[62]) have been compared with selected DFT methods. In particular, we chose two hybrid functionals, B3LYP[63] and B2PLYP,[64−66] which are well-known to provide very good gas-phase molecular properties,[63,66−68] and the conventional PBE functional,[69] which has been shown to provide solvation energies in very good agreement with experimental data.[55,70] Furthermore, the set of parameters employed by the DFTBA method has been originally fitted to the latter functional. In conjunction with these functionals, we employed the 6-31G(d), 6-31G(d,p), and aug-cc-pVTZ (AVTZ) basis sets. In general, PCM calculations have been performed using Universal Force Field cavities with van der Waals atomic radii, scaled by a factor α = 1.1. Different choices of cavity parameters will be explicitly indicated in the next sections. The DFTB/PCM scheme has

Table 1. Solvation Energies and Electrostatic Potential of a Water Molecule in Aqueous Solution[a]

	SE				SE0				MAE($\mathbf{V}^0$)		
α	B3LYP/AVTZ	PBE/AVTZ	PBE/STO-3G	DFTBA	B3LYP/AVTZ	PBE/AVTZ	PBE/STO-3G	DFTBA	PBE/AVTZ	PBE/STO-3G	DFTBA
0.5	−22.20	−21.94	−19.10	−36.25	−22.04	−21.80	−21.32	−32.70	0.0037	0.0640	0.1682
0.6	−15.72	−15.25	−12.90	−16.66	−15.67	−15.12	−14.68	−16.27	0.0022	0.0345	0.0740
0.7	−12.31	−11.88	−8.51	−9.80	−12.28	−11.78	−9.86	−9.72	0.0015	0.0191	0.0339
0.8	−9.42	−9.08	−5.73	−6.40	−9.40	−9.00	−6.66	−6.40	0.0012	0.0127	0.0189
0.9	−7.12	−6.86	−3.97	−4.47	−7.11	−6.81	−4.66	−4.49	0.0010	0.0104	0.0128
1.0	−5.36	−5.17	−2.87	−3.27	−5.36	−5.13	−3.38	−3.30	0.0008	0.0086	0.0096
1.1	−4.07	−3.92	−2.16	−2.48	−4.06	−3.89	−2.54	−2.51	0.0007	0.0072	0.0076
1.2	−3.13	−3.02	−1.67	−1.92	−3.12	−2.99	−1.96	−1.95	0.0006	0.0059	0.0062
1.3	−2.44	−2.36	−1.32	−1.53	−2.44	−2.33	−1.55	−1.55	0.0005	0.0049	0.0051

[a]SE are the solvation energies (kcal/mol), SE0 are the solvation energies calculated on gas-phase B3LYP/AVTZ geometry (kcal/mol), α is the cavity scaling factor, MAE(V0) is reported in atomic units (see paragraph 4.1 for the definition).

been implemented in a localy modified development version of the Gaussian Code (namely GDV.H21).[71] Anharmonic frequency calculations have been performed using the second order perturbative (VPT2) vibrational approach.[49−51]

4. RESULTS AND DISCUSSION

4.1. Energetics. The Solvation Energy (SE) for a given molecule can be defined, to a first approximation, as the difference between the total energy of the molecule optimized in a vacuum and the free energy of solvation of the molecule optimized in solvent. Such an approach is formally exact, under the assumption that solvent effects do not significantly influence the rotational and vibrational degrees of freedom of the molecule. The free energy of solvation for DFT methods is calculated as in eq 2, using the electrostatic potential of eq 7. On the other side, the DFTBA method employs the formulas discussed in the previous section for the energy (eq 14) and for the molecular potential (eq 27). Furthermore the minimal basis set approximation is employed, and the parameters of DFTBA have been fitted to PBE data. In order to separate the effects due to the different approximations in the DFTBA/PCM scheme, in Table 1 a set of values of SEs for a water molecule in aqueous solution have been reported, as computed with B3LYP/AVTZ, PBE/AVTZ, PBE/STO-3G, and DFTBA methods. We used different scaling factors (α) in order to modify the cavity radii and computed the SE for nine values of α, ranging from 0.5 to 1.3. In Figure 1, the energies have also been plotted for a more clear visualization. The SEs computed at the B3LYP/AVTZ and PBE/AVTZ levels are nearly identical for every value of α, suggesting that the effects due to the different exchange-correlation functionals should be very small. A more sensible difference has been found between the PBE/AVTZ and the PBE/STO-3G SEs. Such a difference is nearly constant when varying the cavity radii and can be attributed to the minimal basis set approximation. The SEs computed at the DFTBA level are very close to PBE/STO-3G for large cavities, then diverge for values of α lower than 0.7. This suggests that for large cavities, the energetics of the DFTBA method is mainly influenced by the minimal basis set approximation, while reducing the cavities the approximations introduced in the definition of the DFTBA molecular potential ($\tilde{V}$), discussed in the previous section, become important. In order to quantitatively compare molecular potentials computed with different methods, we estimated the Solvation Energies (SE0) by single point calculations at fixed geometry (i.e., a water molecule in the gas phase optimized at the B3LYP/AVTZ level), without any further optimization. In Table 1, the SE0

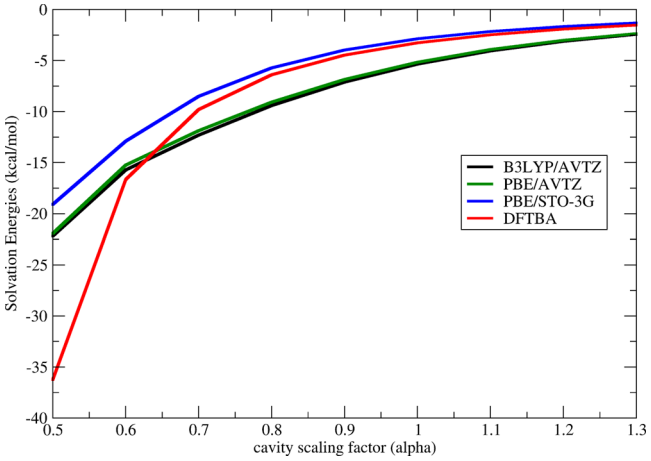

Figure 1. Solvation energies (kcal/mol) of a water molecule in aqueous solution, computed with four different computational methods and plotted as functions of the cavity scaling factor.

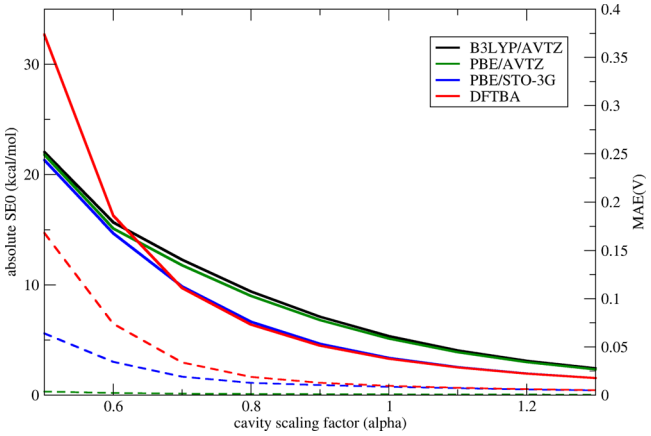

Figure 2. Straight lines refer to the absolute values of the solvation energies at fixed geometry (SE0) of a water molecule in aqueous solution (y axis on the left), as computed at the B3LYP/AVTZ, PBE/AVTZ, PBE/STO-3G, and DFTBA levels. Corresponding values of MAE($\mathbf{V}^0$), computed with respect to B3LYP/AVTZ electrostatic potential, have been reported as dotted lines (y axis on the right). See paragraph 4.1 for details about the definitions of SE0 and MAE($\mathbf{V}^0$), and see Table 1 for numerical values.

dx.doi.org/10.1021/ct301050x | J. Chem. Theory Comput. 2013, 9, 2052−2071

Table 2. SEs for a Set of Organic Molecules in Aqueous Solution (kcal/mol)[a]

	solvation energies (kcal/mol)									
solute	DFTBA		PBE/ STO-3G	PM6	AM1	PBE/ 6-31G(d)	B2PLYP/ 6-31G(d)	B3LYP/ 6-31G(d)	B3LYP/ 6-31G(d,p)	B3LYP/ AVTZ
α	1.1	0.8/0.9	1.1	1.1	1.1	1.1	1.1	1.1	1.1	1.1
methane	−0.04	−0.12	−0.13	−0.17	−0.03	−0.14	−0.11	−0.11	−0.11	−0.12
ethene	−0.24	−0.56	−0.37	−0.40	−0.27	−0.80	−0.81	−0.75	−0.72	−0.78
benzene	−0.63	−1.34	−0.85	−1.35	−1.19	−1.80	−1.88	−1.66	−1.60	−1.55
ammonia	−0.74	−1.91	−3.06	−4.44	−2.96	−3.86	−3.90	−3.82	−3.60	−3.08
methylamine	−0.58	−1.57	−2.43	−3.94	−2.40	−2.85	−2.97	−2.86	−2.72	−2.61
ethylamine	−0.55	−1.56	−2.40	−3.68	−2.44	−2.84	−3.00	−2.86	−2.71	−2.70
piperidine	−0.42	−1.31	−1.93	−3.06	−1.96	−2.07	−2.27	−2.11	−2.03	−2.21
pyridine	−1.04	−2.41	−1.96	−3.63	−2.67	−2.97	−3.33	−3.04	−3.01	−3.28
pyrazine	−1.18	−2.94	−2.37	−4.71	−3.45	−3.15	−3.62	−3.32	−3.33	−3.69
water	−2.48	−4.47	−2.16	−4.12	−3.14	−4.49	−4.83	−4.61	−4.39	−4.07
methanol	−1.94	−3.62	−1.53	−3.56	−2.30	−2.98	−3.38	−3.15	−3.05	−3.13
ethanol	−1.94	−3.76	−1.53	−3.76	−2.31	−2.85	−3.20	−2.99	−2.89	−3.07
acetaldehyde	−2.39	−4.23	−1.04	−5.23	−3.57	−2.97	−3.77	−3.28	−3.30	−4.01
acetone	−2.91	−5.09	−1.21	−5.42	−3.55	−3.38	−4.08	−3.65	−3.67	−4.45
acetic ac.	−3.47	−6.85	−1.84	−5.26	−4.01	−3.87	−4.61	−4.16	−4.14	−4.57
THF	−1.69	−3.18	−1.09	−3.48	−2.09	−1.92	−2.38	−2.22	−2.26	−2.43
furan	−0.75	−1.61	−0.85	−1.48	−1.62	−1.90	−2.13	−1.90	−1.87	−1.89
phenol	−1.91	−3.77	−2.36	−3.53	−2.81	−4.07	−4.33	−4.01	−3.88	−3.76
MAE(neutral)	1.47	0.67	1.24	0.68	0.48	0.38	0.26	0.28	0.24	
NH_4^+	−73.23	−86.99	−72.07	−73.32	−73.32	−72.50	−72.72	−72.61	−72.66	−72.77
OH^-	−85.48	−105.95	−81.63	−87.65	−85.06	−85.18	−85.77	−85.33	−85.17	−80.14
H_3O^+	−77.07	−90.51	−78.38	−78.52	−79.10	−78.04	−78.08	−78.01	−77.76	−77.61
NH_3^+	−74.68	−90.65	−73.65	−75.11	−75.03	−74.28	−74.48	−74.38	−74.39	−74.50
MAE(ions)	1.63	17.27	0.95	2.39	1.87	1.49	1.54	1.47	1.35	

[a] α = 0.8/0.9 indicates that a value of 0.9 has been used for H, C, and O, and a value of 0.8 for N.

Table 3. Total Dipole Moments (Debye) for a Set of Organic Molecules in a Vacuum

	total dipole moments in a vacuum (Debye)								
solute	DFTBA	PBE/STO-3G	PM6	AM1	PBE/6-31G(d)	B2PLYP/6-31G(d)	B3LYP/6-31G(d)	B3LYP/6-31G(d,p)	B3LYP/AVTZ
ammonia	0.86	1.98	2.25	1.85	1.94	1.94	1.91	1.85	1.49
methylamine	0.65	1.70	2.03	1.49	1.47	1.53	1.47	1.42	1.29
ethylamine	0.67	1.71	2.05	1.55	1.44	1.51	1.44	1.39	1.27
piperidine	0.53	1.49	1.85	1.37	1.17	1.28	1.18	1.15	1.18
pyridine	1.15	2.00	2.35	1.97	2.15	2.28	2.19	2.18	2.26
water	1.63	1.55	2.07	1.86	2.07	2.16	2.10	2.04	1.85
methanol	1.47	1.30	2.05	1.62	1.63	1.81	1.69	1.66	1.66
ethanol	1.36	1.24	1.91	1.55	1.50	1.67	1.56	1.53	1.58
acetaldehyde	2.35	1.56	3.21	2.69	2.54	2.86	2.64	2.65	2.88
acetone	2.65	1.71	3.51	2.92	2.73	3.02	2.82	2.83	3.08
acetic ac.	1.77	0.87	2.07	1.89	1.53	1.68	1.58	1.61	1.78
THF	1.68	1.27	2.28	1.92	1.49	1.91	1.79	1.66	1.65
furan	0.04	0.18	0.34	0.49	0.55	0.75	0.63	0.63	0.67
phenol	1.12	1.31	1.36	1.23	1.34	1.41	1.35	1.34	1.27
average	1.28	1.42	2.10	1.74	1.68	1.84	1.74	1.71	1.71
MAE	0.43	0.53	0.43	0.17	0.18	0.16	0.15	0.12	

have been reported as calculated by the mentioned methods. Now, for each α value and indipendently on the particular computational method employed, the vectors of the molecular potential at fixed geometry ($\mathbf{V}^0$) have the same number of elements, and the coordinates of the surface elements are identical. The Mean Absolute Error (MAE) of PBE/AVTZ, PBE/STO-3G, and DFTBA potentials with respect to B3LYP/AVTZ calculations, MAE($\mathbf{V}^0$), can then be computed, averaging the errors of each element of $\mathbf{V}^0$ over all the surface elements. The MAE($\mathbf{V}^0$) have been reported in Table 1 in atomic units. Furthermore, the values of the MAE($\mathbf{V}^0$) and the absolute values of the SE0s have been plotted together in Figure 2 for a visual comparison. From Figure 2, it is evident that the approximations made in the PCM integrals (eq 24) become important only for very small values of the cavity radii, while in a wide range of distances the agreement between DFTBA and PBE/STO-3G is quantitative, both for the energies and the potential. Moreover, we should remember that for small cavities, the errors related to the molecular potential affect also the standard DFT methods, as long as the

dx.doi.org/10.1021/ct301050x | J. Chem. Theory Comput. 2013, 9, 2052−2071

Table 4. Total Dipole Moments (Debye) for a Set of Organic Molecules in Aqueous Solution[a]

	total dipole moments in aqueous solution (Debye)									
solute	DFTBA		PBE/ STO-3G	PM6	AM1	PBE/ 6-31G(d)	B2PLYP/ 6-31G(d)	B3LYP/ 6-31G(d)	B3LYP/ 6-31G(d,p)	B3LYP/ AVTZ
α	1.1	0.8/0.9	1.1	1.1	1.1	1.1	1.1	1.1	1.1	1.1
ammonia	0.90	0.97	2.05	2.42	1.93	2.19	2.18	2.16	2.09	1.90
methylamine	0.72	0.78	1.81	2.28	1.67	1.76	1.83	1.76	1.71	1.73
ethylamine	0.75	0.82	1.84	2.32	1.73	1.76	1.83	1.75	1.71	1.75
piperidine	0.63	0.71	1.66	2.19	1.61	1.52	1.63	1.53	1.50	1.69
pyridine	1.48	1.78	2.34	3.04	2.55	2.82	2.97	2.87	2.86	3.12
water	1.73	1.81	1.64	2.22	1.98	2.29	2.38	2.31	2.26	2.16
methanol	1.64	1.76	1.41	2.31	1.82	1.90	2.10	1.97	1.94	2.05
ethanol	1.59	1.74	1.37	2.26	1.82	1.83	2.03	1.91	1.87	2.06
acetaldehyde	2.88	3.24	1.75	4.13	3.34	3.15	3.52	3.26	3.27	3.71
acetone	3.31	3.76	1.94	4.62	3.68	3.49	3.82	3.57	3.60	4.09
acetic ac.	2.27	2.66	1.01	2.61	2.27	1.93	2.10	1.99	2.02	2.34
THF	1.94	2.15	1.42	2.74	2.24	2.14	2.35	2.20	2.21	2.43
furan	0.02	0.03	0.18	0.46	0.58	0.67	0.93	0.78	0.78	0.87
phenol	1.45	1.63	1.63	1.76	1.60	1.76	1.81	1.75	1.73	1.71
average	1.52	1.70	1.57	2.53	2.06	2.09	2.25	2.13	2.11	2.26
MAE	0.74	0.60	0.73	0.34	0.20	0.24	0.14	0.20	0.19	

[a] α = 0.8/0.9 indicates a value of 0.9 has been used for H, C, and O and a value of 0.8 for N.

Table 5. Mean Absolute Errors (cm^{-1}) of Harmonic Frequencies of a Set of Organic Molecules in a Vacuum, with Respect to B3LYP/AVTZ Results

MAE of harmonic frequencies in vacuum				
solute	DFTBA	PM6	AM1	PBE/6-31G(d)
acetaldehyde	76	152	71	28
acetic ac.	60	195	78	30
acetone	55	152	56	25
ammonia	42	374	83	78
benzene	74	114	41	33
ethanol	69	213	72	31
ethene	107	187	47	37
ethylamine	61	191	60	31
furan	81	128	64	33
methane	48	253	70	16
methanol	86	257	83	44
methylamine	73	234	67	37
phenol	62	123	66	35
piperidine	68	139	49	27
pyrazine	103	110	46	36
pyridine	85	109	43	35
thf	76	150	62	30
water	91	948	289	125
MAE	73	224	75	39

Table 6. Mean Absolute Errors (cm^{-1}) of Harmonic Frequencies of a Set of Organic Molecules in Aqueous Solution, with Respect to B3LYP/AVTZ[a]

MAE of harmonic frequencies in aqueous solution					
solute	DFTBA		PM6	AM1	PBE/6-31G(d)
α	1.1	0.8/0.9	1.1	1.1	1.1
acetaldehyde	75	75	162	67	29
acetic ac	58	61	205	80	30
acetone	53	56	161	52	26
ammonia	44	46	392	105	80
benzene	74	73	116	40	32
ethanol	67	67	203	73	31
ethene	107	108	189	47	37
ethylamine	59	58	194	61	29
furan	79	79	131	61	32
methane	41	42	260	69	17
methanol	86	88	267	83	43
methylamine	70	70	239	71	35
phenol	62	61	125	66	34
piperidine	67	66	140	49	27
pyrazine	103	99	116	48	36
pyridine	85	82	113	41	35
thf	75	72	157	65	29
water	91	97	932	287	116
MAE	72	72	228	76	39

[a] α = 0.8/0.9 indicates a value of 0.9 has been used for H, C, and O and a value of 0.8 for N.

tails of the electronic densities are nonzero beyond the surface, where the integrals are evaluated.

In Table 2, the SEs for a set of 18 neutral molecules and four ions have been reported, as calculated at the DFTBA level, with other semiempirical methods (AM1 and PM6), PBE/STO-3G, and other popular DFT methods. All the MAEs reported in Table 2 have been computed with respect to B3LYP/AVTZ energies. In analogy with the previous discussion about the water molecule, we observe that the SEs at the DFTBA level are comparable to those at the PBE/STO-3G level, being the overall MAE of the DFTBA method for neutral molecules (1.47 kcal/mol), similar to PBE/STO-3G (1.24 kcal/mol). For a direct comparison between computed and experimental SEs, the effects due to electrostatic, cavitation, and dispersion-repulsion interactions should be included[70] in the calculations. In the implementation of DFTB with the COSMO model[52] (DFTB/COSMO), Elstner et al. fitted the atomic cavity parameters in order to reproduce the experimental SEs, obtaining a final RMS error of 1.1 kcal/mol. Similar procedures have been used also in other solvation models developed for the DFTB method. In particular, the Poisson−Boltzmann model (DFTB/PB[53]) showed Mean Unsigned Errors with respect to an experimental SE of 1.7 and 1.9 kcal/mol, for two

dx.doi.org/10.1021/ct301050x | J. Chem. Theory Comput. 2013, 9, 2052−2071

Table 7. Harmonic Frequencies and Solvatochromic Shifts (cm^{-1}) for a Set of Selected Modes of Organic Molecules in Aqueous Solution[a]

		solvent shifts						absolute errors					
mode	solute	DFTBA		PM6	AM1	PBE/ 6-31G(d)	B3LYP/AVTZ	DFTBA		PM6	AM1	PBE/ 6-31G(d)	
	α	1.1	0.8/0.9	1.1	1.1	1.1	1.1	1.1	0.8/0.9	1.1	1.1	1.1	
C=O	acetaldehyde	−43	−76	−56	−30	−28	−41	2	35	15	11	13	
	acetic ac.	−57	−100	−65	−37	−35	−52	5	48	13	15	17	
	acetone	−42	−76	−69	−31	−30	−45	3	31	24	14	15	
	average	−47	−84	−63	−32	−31	−46	3	38	17	13	15	
N−H	ammonia	−6	−13	−7	−6	−11	−14	8	1	7	8	3	
		−6	−14	−25	−17	−11	−14	8	0	11	3	3	
		−5	−12	−25	−18	1	−5	0	7	20	13	6	
	methylamine	−2	−6	−11	−9	−9	−15	13	9	4	6	6	
		−2	−6	−21	−16	−3	−9	7	3	12	7	6	
	ethylamine	−2	−5	−13	−5	−9	−15	13	10	2	10	6	
		−2	−6	−18	−11	−3	−9	7	3	9	2	6	
	piperidine	1	2	−14	−5	−5	−12	13	14	2	7	7	
	average	−3	−8	−17	−11	−6	−12	9	6	8	7	5	
O−H	water	−23	−40	−1	−11	−13	−28	5	12	27	17	15	
		−18	−34	−46	−22	6	−14	4	20	32	8	20	
	methanol	−10	−21	0	−15	0	−15	5	6	15	0	15	
	ethanol	−10	−20	0	−17	−1	−16	6	4	16	1	15	
	phenol	−8	−18	−10	−31	−10	−24	16	6	14	7	14	
	average	−14	−27	−12	−19	−6	−19	7	10	21	7	16	

[a]Absolute errors have been computed with respect to B3LYP/AVTZ results.

different benchmark sets of molecules; finally, using the generalized Born model (DFTB/GBSA[54]), Liu et al. obtained a final MAD of 1.11 kcal/mol. In both of these two latter implementations, the atomic parameters defining the cavities and the surface tension parameters were fitted in order to reproduce the experimental energies. A fitting procedure similar to that employed by Elstner et al. could be in principle applied also to the DFTB/PCM model, in order to improve the energetics of solvation. Preliminary calculations showed that an energetics closer to DFT can be obtained by tuning the cavity radii. In particular, in Table 2, we note that when a reduced value of α is used (0.9 for hydrogen, carbon, and oxygen atoms and of 0.8 for nitrogen atoms), the accuracy of the SEs of the neutral molecules is improved, resulting in an overall MAE of just 0.67 kcal/mol with respect to B3LYP/AVTZ calculations. It is worth it to note that the present empirical correction does not improve at the same time the SEs of both the neutral and ionic systems. More in general, the parameters defining the PCM cavities are very sensitive to the total charge of the solute, to the hybridization of the atoms, and to substituent effects, and targeted studies are necessary in order to obtain a high accuracy in the energetics of solvation (see for example the discussion about the optimization of the cavity parameters for the UAHF model[57] and references therein).

4.2. Dipole Moments. In Table 3, the total dipole moments in a vacuum, as computed with different methods, are reported. It is known that the minimal basis set approximation usually affects the accuracy of the DFTB dipole moments when calculated from the Mulliken atomic charges.[19,48] This is confirmed in our computations, where the MAE of the dipole moments of DFTBA and PBE/STO-3G are very similar, being respectively 0.43 and 0.53 D. It has been shown that use of Lowdin charges leads only to a marginal refinement,[48] and for an effective treatment of the electrostatics, more accurate methods, such as the CM3 proposed by Truhlar et al.,[47,48] should be used. A new generation of DFTB methods is under development, based on the use of the CM3 charges in place of the Mulliken charges in the SCF, and on a third order expansion of the total energy on charge fluctuations, in order to provide an improved electrostatic description at the DFTB level (see, e.g., Spiegelman et al.,[44,46,72] York and Giese,[73,74] and Elstner et al.[75−77]). Hence, a detailed discussion about the accuracy of the dipole moments is far beyond the aim of this work. We just remark here that at variance from the CM3 method, our implementation (eq 33) does not require any additional parametrization and leads to a MAE of the dipole moments in very good agreement with the other implementations based on the Mulliken charges. In particular, Sattelmeyer et al.[19] obtained a MAE of ∼0.4 D, averaging the errors of the DFTB dipole moments with respect to MP2/cc-pVTZ calculations, over a set of 47 organic molecules; Truhlar et al.[48] found a value of 0.56 D calculating the errors with respect to the experimental dipole moments of a set of 219 molecules. The accuracy of our results is also in good agreement with the work of Liu et al.,[54] where the DFTB dipole moments have been compared to B3LYP/6-31G* calculations. On average, our calculations suggest that DFTBA dipoles have an accuracy comparable to PM6 calculations and slightly lower than AM1. This is in line with the results reported by Stewart,[61] who found an average error of 0.38 D for PM6 and 0.26 D for AM1 calculations, with respect to the experimental dipole moments. When molecules in aqueous solution are considered (see Table 4), the interaction between the solute electronic densities and the solvent charge distribution leads to larger dipole moments. For PM6, AM1, and DFT methods, the mean increment of the dipole moments due to the solvent is about 0.4 D. In the case of DFTBA with standard cavities, the dipole moments in water are underestimated by about 0.7 D with respect to B3LYP/AVTZ, resembling the behavior of PBE/STO-3G. Also in this case, similarly to the SE, reduced values of the cavity radii lead

Table 8. Harmonic, Anharmonic (GVPT2) Frequencies and Anharmonic Shifts in cm^{-1} of Acetaldehyde[a]

harmonic frequencies								
modes	symm.	DFTBA	PM6	AM1	PBE/6-31G(d)	B3LYP/AVTZ	exptl.[b]	assignments
1	A′	3027 (110)	2789 (348)	3154 (16)	3106 (31)	3134 (3)	3138	CH_3 stretching
11	A″	2996 (76)	2691 (380)	3089 (16)	3041 (31)	3072 (0)	3072	CH_3 stretching
2	A′	2871 (185)	2691 (365)	3062 (6)	2978 (78)	3021 (34)	3056	CH_3 stretching
3	A′	2472 (369)	2645 (196)	3057 (216)	2794 (47)	2868 (27)	2841	CH stretching
4	A′	1740 (33)	1795 (20)	2059 (285)	1787 (13)	1805 (30)	1774	C═O stretching
12	A″	1424 (45)	1315 (153)	1426 (43)	1449 (20)	1469 (0)	1469	CH_3 bending
5	A′	1422 (34)	1279 (177)	1380 (76)	1440 (16)	1459 (2)	1457	CH_3 bending
6	A′	1405 (5)	1228 (182)	1372 (38)	1398 (12)	1421 (10)	1411	CH bending
7	A′	1353 (46)	1211 (188)	1358 (41)	1346 (54)	1379 (20)	1400	CH_3 flip
13	A″	1124 (20)	1145 (0)	1218 (72)	1102 (43)	1135 (9)	1145	CH oop bending
8	A′	1062 (67)	1082 (47)	1118 (11)	1099 (30)	1129 (0)	1129	
9	A′	950 (43)	984 (78)	1033 (126)	870 (36)	886 (20)	906	CC stretching
14	A″	743 (37)	804 (23)	814 (33)	747 (33)	774 (5)	780	
10	A′	515 (5)	489 (31)	521 (0)	491 (29)	509 (11)	521	
15	A″	121	70	93	153	157		
MAE		77	156	70	34	12	0	
anharmonic frequencies								
modes	symm.	DFTBA	PM6	AM1	PBE/6-31G(d)	B3LYP/AVTZ	exptl.[b]	assignments
1	A′	2923 (90)	2762 (251)	3058 (43)	2954 (60)	2991 (22)	3014	CH_3 stretching
11	A″	2904 (59)	2649 (314)	2976 (11)	2894 (69)	2933 (31)	2964	CH_3 stretching
2	A′	2820 (102)	2650 (272)	2965 (41)	2870 (52)	2917 (5)	2923	CH_3 stretching
3	A′	2417 (297)	2616 (99)	2963 (248)	2591 (123)	2673 (42)	2715	CH stretching
4	A′	1728 (17)	1776 (30)	2033 (287)	1762 (16)	1780 (34)	1746	C═O stretching
12	A″	1386 (50)	1298 (137)	1396 (39)	1407 (28)	1426 (9)	1436	CH_3 bending
5	A′	1387 (45)	1264 (168)	1350 (82)	1400 (32)	1421 (12)	1433	CH_3 bending
6	A′	1379 (15)	1200 (194)	1343 (51)	1370 (24)	1396 (1)	1394	CH bending
7	A′	1326 (25)	1191 (161)	1335 (17)	1313 (39)	1345 (6)	1352	CH_3 flip
13	A″	1103 (10)	1122 (8)	1191 (77)	1077 (36)	1111 (2)	1113	CH oop bending
8	A′	1042 (55)	1076 (21)	1107 (10)	1075 (22)	1104 (6)	1097	
9	A′	946 (80)	986 (120)	1026 (160)	831 (34)	852 (13)	865	CC stretching
14	A″	734 (29)	797 (33)	805 (40)	734 (29)	762 (1)	764	
10	A′	516 (7)	489 (19)	521 (12)	491 (17)	511 (2)	508	
15	A″	108	52	82	140	143	144	
MAE		63	131	80	41	13	0	
anharmonic shifts								
modes	symm.	DFTBA	PM6	AM1	PBE/6-31G(d)	B3LYP/AVTZ	exptl.[b]	assignments
1	A′	−104	−27	−96	−152	−142	−123	CH_3 stretching
11	A″	−92	−42	−113	−147	−139	−108	CH_3 stretching
2	A′	−50	−40	−97	−108	−104	−133	CH_3 stretching
3	A′	−55	−29	−94	−202	−195	−126	CH stretching
4	A′	−11	−18	−26	−25	−24	−28	C═O stretching
12	A″	−38	−17	−29	−41	−42	−33	CH_3 bending
5	A′	−34	−14	−29	−39	−38	−23	CH_3 bending
6	A′	−26	−28	−29	−27	−25	−16	CH bending
7	A′	−26	−20	−22	−32	−33	−47	CH_3 flip
13	A″	−21	−22	−27	−25	−24	−31	CH oop bending
8	A′	−20	−6	−10	−24	−24	−32	
9	A′	−3	1	−6	−38	−34	−40	CC stretching
14	A″	−8	−7	−9	−13	−12	−16	
10	A′	0	0	0	0	1	−12	
15	A″	−12	−18	−10	−13	−13		
hybrid frequencies: B3LYP/AVTZ harmonics + anharmonic shifts								
modes	symm.	DFTBA	PM6	AM1	PBE/6-31G(d)	B3LYP/AVTZ	exptl.[b]	assignments
1	A′	3030 (15)	3106 (92)	3037 (23)	2981 (32)	2991 (22)	3014	CH_3 stretching
11	A″	2980 (16)	3030 (65)	2959 (4)	2925 (38)	2933 (31)	2964	CH_3 stretching
2	A′	2971 (48)	2980 (57)	2924 (0)	2913 (9)	2917 (5)	2923	CH_3 stretching
3	A′	2813 (98)	2839 (124)	2774 (58)	2666 (49)	2673 (42)	2715	CH stretching
4	A′	1793 (47)	1786 (40)	1778 (32)	1779 (33)	1780 (34)	1746	C═O stretching

dx.doi.org/10.1021/ct301050x | J. Chem. Theory Comput. 2013, 9, 2052−2071

Table 8. continued

hybrid frequencies: B3LYP/AVTZ harmonics + anharmonic shifts								
modes	symm.	DFTBA	PM6	AM1	PBE/6-31G(d)	B3LYP/AVTZ	exptl.[b]	assignments
12	A″	1431 (5)	1451 (15)	1439 (3)	1427 (8)	1426 (9)	1436	CH_3 bending
5	A′	1425 (8)	1445 (12)	1430 (3)	1420 (12)	1421 (12)	1433	CH_3 bending
6	A′	1395 (0)	1393 (1)	1392 (2)	1394 (0)	1396 (1)	1394	CH bending
7	A′	1352 (0)	1358 (6)	1356 (3)	1346 (5)	1345 (6)	1352	CH_3 flip
13	A″	1114 (0)	1113 (0)	1108 (5)	1110 (3)	1111 (2)	1113	CH oop bending
8	A′	1109 (11)	1122 (25)	1119 (21)	1105 (7)	1104 (6)	1097	
9	A′	882 (16)	887 (21)	879 (13)	847 (18)	852 (13)	865	CC stretching
14	A″	766 (2)	767 (3)	765 (1)	761 (2)	762 (1)	764	
10	A′	509 (1)	509 (1)	509 (0)	510 (1)	511 (2)	508	
15	A″	144	139	146	144	143	144	
MAE		19	33	12	16	13	0	

[a]In parentheses, the absolute errors with respect to experimental frequencies. Mean Absolute Errors (MAE) for harmonic and anharmonic frequencies have been computed with reference to experimental frequencies. Mode 15 has been neglected in the MAE calculation due to the lack of experimental harmonic frequency. Hybrid frequencies have been calculated by summing the harmonic frequencies at the B3LYP/AVTZ level to the anharmonic shifts of each method. [b]Experimental harmonic and anharmonic frequencies from measurement on gas-phase acetaldehyde performed by Wiberg et al.[88]

to an improvement of results (the MAE of DFTBA calculations using α = 0.8/0.9 is reduced to 0.60 D).

4.3. Harmonic Frequencies. In Table 5, the MAEs of the harmonic frequencies of each molecule in a vacuum, computed with respect to B3LYP/AVTZ calculations, have been reported. We observe that DFTBA and AM1 are the most effective semiempirical methods for the computation of harmonic frequencies, with a MAE of about 70 cm^{-1} in both cases, while the PM6 method shows a sensibly lower accuracy (MAE of 224 cm^{-1}). As widely disscussed in the Introduction, we recall that the computation of vibrational frequencies at the DFTB level is a field of large interest, and special parametrizations[37−39,76] have been developed in past years in order to fit the DFTB harmonic frequencies to the experimental fundamentals, at the price of a reduced accuracy of the energetics. Unfortunately, a successful case in which the energetics and the vibrational properties were accurately reproduced with the same set of parameters has not yet been reported in the literature, and at the moment the most used parameters are designed in order to reproduce only selected molecular properties.

Harmonic frequencies for the same set of molecules in aqueous solution are reported in Table 6. We note that the overall accuracy is very similar in solvent as in vacuum calculations for all the employed methods, and again DFTBA and AM1 approaches provide a better agreement with DFT than PM6. By the way, solvation effects are relevant for just a few specific modes, being negligible for most of the other vibrations. For this reason, an analysis of the frequency shifts of such modes is more meaningful than the analysis of the overall MAE.

In Table 7, the solvatochromic shifts of the C═O, N−H, and O−H stretching modes in aqueous solution are reported as calculated with different methods. We note that for these modes solvent effects are significant, with shifts at the B3LYP/AVTZ level of about 46 cm^{-1} for C═O stretching modes, 12 cm^{-1} for N−H stretching modes, and 19 cm^{-1} for O−H stretching modes. Among the semiempirical methods, DFTBA with standard cavities is the most accurate method in the reproduction of such shifts. In particular, the solvent shifts of the C═O stretching modes are reproduced with errors lower than 5 cm^{-1} for acetaldehyde, acetic acid, and acetone molecules. This is the most accurate result among either of the other semiempirical methods and also when compared with the PBE/6-31G(d) method. Analogously, the average errors affecting the shifts of the N−H and O−H stretching modes are smaller than 9 and 7 cm^{-1}, respectively. The maximum error of DFTBA calculations is related to the solvatochromic shift of the O−H stretching mode of phenol, and it is just 16 cm^{-1}, much lower than the maximum errors of PM6 (32 cm^{-1}) and PBE/6-31G(d) (20 cm^{-1}) methods and comparable with the maximum error of the AM1 method (17 cm^{-1}). In this respect, we recall that, for aromatic molecules and conjugated systems, effects due to the lack of diffuse functions, self-interaction error, and overpolarization are known to affect the DFTB treatment.[43,78−80]

As a final remark about harmonic frequency calculations, we point out that the calculations with standard cavities seem to be more reliable than the calculations with reduced cavities for vibrational properties. In particular, we note that the average errors on the solvatochromic shifts of C═O stretching modes are 3 cm^{-1} for α = 1.1 and 38 cm^{-1} for α = 0.8/0.9. Another analogous case is the shift of the O−H stretching modes of the water molecule, which are sensibly better using α = 1.1 than α = 0.8/0.9. This suggests that a fitting procedure of the cavity parameters, similar to those employed in the DFTB/COSMO,[52] DFTB/PB,[53] and DFTB/GBSA[54] implementations, could lead to an improved enegetics of solvation, at the price of a reduced accuracy for the vibrational properties. This is true in particular for the schemes which employ a low number of parameters, as our present case. So in our approach, we prefer to avoid any fitting procedure, in order to have more flexibility in the calculations of the spectroscopical properties.

4.4. Test Case: Anharmonic Vibrational Frequencies of Acetic Acid and Acetaldehyde in the Gas Phase. In the VPT2 framework, it has been shown that the anharmonic corrections are usually similar when computed with different computational approaches,[51,66,81] and hybrid schemes coupling different DFT methods or Coupled Cluster (CC) and DFT have been found to provide very accurate vibrational properties when compared to experimental data, at reasonable computational cost.[67,82,83] In particular, for the uracil molecule,[82] a CC/DFT hybrid scheme—where the anharmonic shifts computed at the DFT level were combined with the CC harmonic

Table 9. Harmonic, Anharmonic (GVPT2) Frequencies and Anharmonic Shifts (cm^{-1}) of Acetic Acid[a]

harmonic frequencies							
modes	symm.	DFTBA	PM6	AM1	PBE/6-31G(d)	B3LYP/AVTZ	assignments
1	A′	3621 (116)	2780 (957)	3429 (307)	3561 (176)	3737	OH stretching
2	A′	3037 (122)	2682 (476)	3152 (7)	3129 (29)	3159	CH_3 stretching
13	A″	3003 (104)	2676 (431)	3068 (39)	3076 (31)	3108	CH_3 stretching
3	A′	2879 (173)	2550 (502)	3057 (5)	3009 (43)	3052	CH_3 stretching
4	A′	1703 (108)	1839 (27)	2087 (275)	1802 (9)	1811	C═O stretching
14	A″	1425 (52)	1319 (158)	1549 (71)	1456 (21)	1477	CH_3 bending
5	A′	1422 (49)	1303 (168)	1429 (42)	1452 (18)	1471	CH_3 bending
6	A′	1388 (19)	1217 (191)	1412 (4)	1381 (27)	1408	CH_3 flip
7	A′	1275 (59)	1203 (131)	1371 (36)	1320 (14)	1334	CO stretching
8	A′	1182 (18)	1147 (53)	1363 (162)	1182 (18)	1201	OH ip bending
15	A″	1027 (42)	1035 (35)	1100 (29)	1037 (33)	1070	
9	A′	991 (7)	1020 (22)	1072 (74)	968 (29)	998	
10	A′	866 (9)	951 (94)	1038 (180)	847 (10)	857	CC stretching
16	A″	588 (74)	593 (70)	589 (74)	682 (19)	663	OH oop bending
11	A′	560 (24)	513 (70)	569 (14)	561 (22)	584	
17	A″	483 (62)	504 (41)	520 (25)	530 (15)	546	
12	A′	401 (22)	375 (48)	418 (5)	406 (17)	424	
18	A″	60 (9)	48 (22)	24 (45)	61 (8)	70	
MAE		59	194	77	30	0	
anharmonic frequencies							
modes	symm.	DFTBA	PM6	AM1	PBE/6-31G(d)	B3LYP/AVTZ	exptl.[b]	assignments
1	A′	3471 (96)	2752 (815)	3337 (230)	3372 (195)	3554 (13)	3568	OH stretching
2	A′	2931 (125)	2643 (413)	3055 (1)	2974 (82)	3015 (41)	3057	CH_3 stretching
13	A″	2908 (98)	2635 (371)	2970 (36)	2920 (86)	2966 (40)	3007	CH_3 stretching
3	A′	2829 (123)	2517 (435)	2964 (11)	2900 (52)	2944 (8)	2953	CH_3 stretching
4	A′	1673 (106)	1831 (51)	2038 (257)	1768 (12)	1779 (0)	1780	C═O stretching
14	A″	1394 (46)	1290 (150)	1513 (72)	1410 (30)	1438 (2)	1441	CH_3 bending
5	A′	1380 (55)	1285 (150)	1402 (33)	1415 (20)	1434 (1)	1436	CH_3 bending
6	A′	1358 (22)	1192 (188)	1385 (4)	1349 (31)	1369 (11)	1381	CH_3 flip
7	A′	1251 (73)	1183 (141)	1338 (13)	1261 (63)	1319 (5)	1325	CO stretching
8	A′	1153 (3)	1083 (66)	1333 (183)	1145 (4)	1155 (5)	1150	OH ip bending
15	A″	1007 (39)	1023 (23)	1093 (46)	1023 (23)	1052 (5)	1047	
9	A′	976 (9)	988 (2)	1051 (65)	953 (32)	980 (5)	986	
10	A′	844 (0)	940 (96)	1024 (180)	829 (14)	839 (4)	844	CC stretching
16	A″	564 (70)	575 (59)	564 (70)	659 (24)	642 (7)	635	OH oop bending
11	A′	555 (22)	513 (64)	571 (6)	553 (24)	576 (1)	577	
17	A″	469 (63)	499 (33)	508 (24)	520 (12)	531 (1)	533	
12	A′	401 (21)	374 (48)	417 (5)	407 (15)	424 (1)	423	
18	A″	52 (50)	31 (71)	−6 (109)	49 (53)	55 (47)	103	
MAE		57	176	75	43	11	0	
anharmonic shifts							
modes	symm.	DFTBA	PM6	AM1	PBE/6-31G(d)	B3LYP/AVTZ	assignments
1	A′	−149	−27	−92	−189	−182	OH stretching
2	A′	−105	−39	−96	−155	−144	CH_3 stretching
13	A″	−95	−41	−98	−156	−142	CH_3 stretching
3	A′	−50	−32	−93	−108	−107	CH_3 stretching
4	A′	−29	−7	−49	−34	−32	C═O stretching
14	A″	−30	−28	−35	−46	−39	CH_3 bending
5	A′	−42	−18	−27	−37	−37	CH_3 bending
6	A′	−30	−24	−27	−31	−38	CH_3 flip
7	A′	−23	−20	−33	−58	−15	CO stretching
8	A′	−29	−63	−30	−37	−45	OH ip bending
15	A″	−19	−11	−6	−14	−17	
9	A′	−14	−32	−21	−14	−17	
10	A′	−21	−11	−14	−17	−18	CC stretching
16	A″	−24	−17	−24	−22	−20	OH oop bending
11	A′	−4	0	1	−8	−8	
17	A″	−14	−4	−11	−10	−14	

dx.doi.org/10.1021/ct301050x | J. Chem. Theory Comput. 2013, 9, 2052−2071

Table 9. continued

anharmonic shifts							
modes	symm.	DFTBA	PM6	AM1	PBE/6-31G(d)	B3LYP/AVTZ	assignments
12	A′	0	0	0	0	0	
18	A″	−7	−16	−31	−11	−15	

hybrid frequencies: B3LYP/AVTZ harmonics + anharmonic shifts								
modes	symm.	DFTBA	PM6	AM1	PBE/6-31G(d)	B3LYP/AVTZ	exptl.[b]	assignments
1	A′	3588 (20)	3710 (142)	3645 (77)	3548 (19)	3554 (13)	3568	OH stretching
2	A′	3053 (3)	3120 (63)	3062 (5)	3004 (52)	3015 (41)	3057	CH_3 stretching
13	A″	3012 (5)	3067 (60)	3010 (3)	2952 (54)	2966 (40)	3007	CH_3 stretching
3	A′	3002 (49)	3019 (66)	2959 (6)	2943 (9)	2944 (8)	2953	CH_3 stretching
4	A′	1782 (1)	1804 (23)	1762 (18)	1777 (3)	1779 (0)	1780	C═O stretching
14	A″	1447 (6)	1449 (8)	1442 (1)	1431 (9)	1438 (2)	1441	CH_3 bending
5	A′	1429 (6)	1453 (17)	1444 (8)	1434 (1)	1434 (1)	1436	CH_3 bending
6	A′	1378 (2)	1383 (2)	1380 (0)	1377 (3)	1369 (11)	1381	CH_3 flip
7	A′	1310 (14)	1314 (10)	1301 (23)	1276 (48)	1319 (5)	1325	CO stretching
8	A′	1171 (21)	1137 (12)	1170 (20)	1163 (13)	1155 (5)	1150	OH ip bending
15	A″	1050 (3)	1058 (11)	1063 (16)	1056 (9)	1052 (5)	1047	
9	A′	983 (2)	966 (19)	977 (8)	983 (2)	980 (5)	986	
10	A′	835 (8)	845 (1)	843 (0)	839 (4)	839 (4)	844	CC stretching
16	A″	639 (4)	645 (10)	638 (3)	640 (5)	642 (7)	635	OH oop bending
11	A′	579 (1)	583 (6)	585 (8)	575 (2)	576 (1)	577	
17	A″	531 (1)	541 (8)	534 (0)	535 (2)	531 (1)	533	
12	A′	424 (1)	423 (0)	423 (0)	424 (1)	424 (1)	423	
18	A″	62 (40)	53 (49)	39 (63)	58 (44)	55 (47)	103	
MAE		10	28	14	15	11		

[a]In parentheses, the absolute errors with respect to experimental frequencies. Mean Absolute Errors (MAE) for anharmonic frequencies have been computed with reference to experimental frequencies. Hybrid frequencies have been calculated by summing the harmonic frequencies at the B3LYP/AVTZ level to the anharmonic shifts of each method. [b]Pettersson et al.[89]

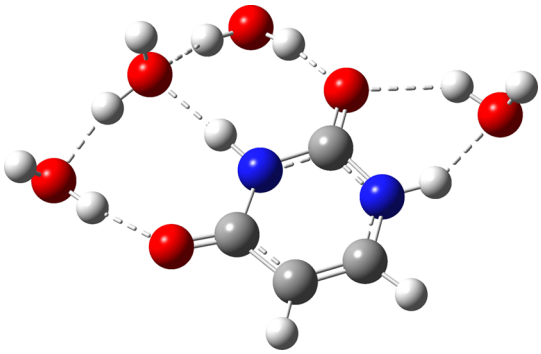

Figure 3. Four explicit water molecules of the first shell of solvation of a uracil molecule in aqueous solution.

frequencies—led to frequencies in very good agreement with experimental results. In analogy with our previous works, we can try to extend such a hybrid scheme from the combination of CC/DFT to the combination of DFT/DFTB methods.

In Tables 8 and 9, the anharmonic shifts computed with different methods have been combined to the B3LYP/AVTZ harmonic frequencies, for acetaldehyde and acetic acid molecules, respectively. For each of these molecules, we note a good overall agreement between hybrid DFT/DFTBA frequencies and experimental fundamentals, with an overall MAE of 19 cm^{-1} for acetaldehyde and 10 cm^{-1} for acetic acid. In the latter case, the performances of the hybrid DFT/DFTBA approach are even better than the DFT/PBE/6-31G(d) approach, which shows a MAE of 16 cm^{-1}. For comparison, an overall MAE of about 10 cm^{-1} was found when the hybrid CC/DFT scheme was applied to the calculation of the frequencies of the uracil molecule,[82] while calculations at the full DFT level for a gas-phase glycine molecule[67] led to a MAE of 11 cm^{-1}. Furthermore, a MAE of 38 cm^{-1} was found when an approximated VPT2 scheme[84] was used in conjuction with full DFT calculations, in order to compute the infrared spectrum of the glycine molecule adsorbed on the (100) surface of silicon.[85] The results obtained at the DFTBA level are even more encouraging if we consider that the MAE can be mainly attributed to large errors localized on a few stretching modes, while all the other vibrations are well reproduced. In particular, the main sources of error for acetaldehyde are two CH stretching modes, whose frequencies differ from the experimental values by 98 and 48 cm^{-1}, respectively, and the C═O stretching mode (error of 47 cm^{-1}). The situation is even better for the acetic acid molecule, for which a significant error (49 cm^{-1}) is found only for one CH stretching mode. Generally speaking, the discrepancies found in DFTBA calculations related to the frequencies of stretching modes of polarized bonds could be attributed to the fair DFTBA electrostatic description of the chemical bonding, based on the Mulliken charges,[48] and on the minimal basis approximation. On the other side, the large errors of the CH stretching modes are very similar to those found by Witek et al.,[18,37] and they can be related to the parameters of the C and H interactions. So we suggest that a reparametrization of the repulsive potentials based on high level harmonic frequencies, rather than on experimental data, could sensibly improve the hybrid frequencies for medium sized systems and could also lead to acceptable anharmonic frequencies at the full DFTBA level, which could be used for very large systems. Finally, we remark that one of the main advantages of our VPT2 approach, compared to other time-independent approaches,[43,44] is that

Table 10. Solvatochromic Shifts for Selected Harmonic Frequencies of Uracil in Aqueous Solution[a]

stretching modes		gas phase	uracil +PCM	uracil +4H_2O	uracil +4H_2O +PCM
1. N−H	DFTBA(0.8/0.9)	3565	3561 (−4)	3233 [−332]	3290 (+57)
	DFTBA(1.1)		3558 (−7)		3203 (−30)
	B3LYP/AN07D	3639	3615 (−24)	3398 [−241]	3395 (−3)
2. N−H	DFTBA(0.8/0.9)	3545	3542 (−3)	3062 [−483]	3068 (+6)
	DFTBA(1.1)		3546 (+1)		3037 (−25)
	B3LYP/AN07D	3595	3589 (−6)	3215 [−380]	3265 (+50)
3. C−H	DFTBA(0.8/0.9)	3050	3051 (+1)	3049 [−1]	3050 (+1)
	DFTBA(1.1)		3052 (+2)		3050 (+1)
	B3LYP/AN07D	3253	3254 (+1)	3253 [0]	3254 (+1)
4. C−H	DFTBA(0.8/0.9)	2970	3008 (+38)	2972 [+2]	3006 (+34)
	DFTBA(1.1)		2999 (+29)		2996 (+24)
	B3LYP/AN07D	3212	3233 (+21)	3214 [+2]	3232 (+18)
5. C═O	DFTBA(0.8/0.9)	1715	1676 (−39)	1704 [−11]	1681 (−23)
	DFTBA(1.1)		1681 (−34)		1684 (−20)
	B3LYP/AN07D	1806	1749 (−57)	1773 [−33]	1729 (−44)
6. C═O	DFTBA(0.8/0.9)	1649	1540 (−109)	1631 [−18]	1539 (−92)
	DFTBA(1.1)		1611 (−38)		1611 (−20)
	B3LYP/AN07D	1771	1696 (−75)	1740 [−31]	1699 (−41)

[a]IEF-PCM model has been used. In round brackets, the solvatochromic shifts due to the PCM model (i.e., the difference of uracil+PCM and uracil +4H_2O+PCM frequencies, with respect to uracil and uracil+4H_2O frequencies, respectively). In square brackets, the solvatochromic shifts due to the inclusion of four explicit water molecules (i.e. the difference of uracil+4H_2O frequencies, with respect to uracil frequencies).

Fermi resonances can be effectively treated by the new HDCPT2 model.[51]

4.5. Test Case: Anharmonic Vibrational Frequencies of Uracil in Aqueous Solution. In Figure 3, the first shell of solvation of uracil in aqueous solution is shown. This model, embedded into the polarizable continuum, has been widely used in the literature (see Improta and Barone[24] and references therein), and it has been adopted here in order to model the spectroscopic properties of solvated uracil.

In Table 10, the harmonic frequencies and solvatochromic shifts of selected stretching modes of uracil, as calculated at the DFTBA and B3LYP/AN07D levels employing different solvent models, are reported. The shifts have been also visualized in Figure 6 by histograms, for a better comparison of results. In this case, we chose the B3LYP/AN07D method as a reference method, because it was found to provide very good results in the computation of vibrational frequencies of the gas-phase uracil molecule.[82] In Table 10, we note that the absolute magnitude of the errors of the DFTBA harmonic frequencies is quite large, in line with the results of Tables 5 and 6. However, it is noteworthy that the solvatochromic shifts of the frequencies calculated at DFTBA and B3LYP/AN07D are in very good qualitative agreement. In particular, when four explicit water molecules are added to the gas-phase uracil molecule (Figure 6, part b), both methods predict that the frequencies of the N−H and C═O stretching modes are red-shifted, while the C−H stretching modes do not undergo any significant shift. When PCM is added to the gas-phase uracil and uracil+4H_2O (Figure 6, part c), the agreement between the DFTBA and B3LYP/AN07D shifts is again reasonable, the shifts being always in the same direction. There is only one case in which the frequency shifts due to the PCM have different signs between DFT and DFTBA calculations: the N−H stretching modes of the uracil+4H_2O+PCM model. This could be due to the fact that the N−H moieties of uracil are involved in the hydrogen bonds with the solvent molecules (see Figure 3), so that polarization effects induced by such molecules, not well described at the DFTBA level, could occur. By the way, the PCM contribution to the total solvatochromic shift is very small, when compared to the shift due to the inclusion of the explicit water molecules, so that the total shift is still in reasonable agreement between DFT and DFTBA calculations, as shown in Figure 6, part a. The overall agreement between DFT and DFTBA solvent shifts suggests that the approach used to compute the hybrid DFT/DFTBA frequencies for gas-phase acetaldehye and acetic acid molecules could be extended to the computation of accurate hybrid frequencies in solution.

In Table 11, the hybrid frequencies of the uracil molecule, obtained adding the anharmonic shifts at the DFTBA level to the B3LYP/AN07D harmonic frequencies, have been reported. For the gas-phase uracil, we observe that the overall MAE, averaged over all normal modes, between hybrid and experimental frequencies is just 19 cm^{-1}, comparable to that observed for acetaldehyde. The experimental spectra of uracil in aqueous solution are available only in the region below 1800 cm^{-1}, due to the strong absorptions of the O−H stretching modes of the solvent water molecules. So we selected nine normal modes, of frequencies between 1800 and 1000 cm^{-1}, and we used the available experimental frequencies for the study of the solvatochromic shifts computed at the DFT/DFTBA level, using different solvation models. If we compare the MAE of uracil+4H_2O (20 cm^{-1}) with the MAE of uracil +PCM (36 cm^{-1}), we note that the inclusion of the four explicit water molecules sensibly improves the agreement with the experimental data. In particular, the C═O stretching modes and the mode 9 (in plane ring distortion) are sensibly improved by the explicit inclusion of water molecules. The MAE of uracil +4H_2O+PCM is 25 cm^{-1}, comparable to uracil+4H_2O. The PCM sensibly improves modes 10, 12, and 13, which are quite delocalized over the uracil molecule. These results seem to indicate that inclusion of some explicit water molecules is necessary in order to correctly compute the frequencies of localized modes, which involve a direct interaction with the potential of the water molecules. The PCM provides a general improvement of the low frequency, delocalized modes.

Table 11. Hybrid DFT/DFTB Frequencies of Uracil in Aqueous Solution[a]

	modes	symm.	exp.[b] (gas-phase)	uracil	uracil +PCM	uracil +4H_2O	uracil +4H_2O +PCM	exptl.[c,d] (water)
1	ν(N−H)	A′	3485	3502 (17)				
2	ν(N−H)	A′	3435	3459 (24)				
3	ν(C−H)	A′	3117[e]	3168 (51)				
4	ν(C−H)	A′	3072[e]	3103 (31)				
5	ν(C═O)	A′	1764	1746 (17)	1689 (18)	1708 (0)	1660 (47)	1708[c]
6	ν(C═O)	A′	1706	1731 (25)	1642 (28)	1685 (14)	1641 (29)	1671[c]
7	ν(C═C)	A′	1643	1608 (34)	1608 (22)	1601 (29)	1599 (31)	1631[c]
8	δ	A′	1472	1444 (27)	1463 (42)	1476 (29)	1470 (35)	1506[d]
9	δ	A′	1400	1346 (53)	1357 (98)	1438 (17)	1431 (24)	1456[d]
10	δ	A′	1389	1362 (26)	1371 (44)	1385 (30)	1394 (21)	1416[d]
11	δ	A′	1359	1358 (0)	1380 (-)	1376 (-)	1380 (-)	
12	δ	A′	1217	1187 (29)	1201 (23)	1206 (18)	1220 (4)	1225[d]
13	δ	A′	1185	1182 (2)	1201 (35)	1203 (33)	1209 (27)	1237[c]
14	δ	A′	1075	1068 (6)	1107 (12)	1086 (8)	1084 (10)	1095[c]
15	γ	A″	987	954 (32)				
16	δ	A′	980	957 (22)				
17	δ	A′	958	947 (10)				
18	γ	A″	804	809 (5)				
19	δ	A′	759	759 (0)				
20	γ	A″	757	762 (5)				
21	γ	A″	718	718 (0)				
22	γ	A″	662	678 (16)				
23	δ	A′	562	550 (11)				
24	γ	A″	551	575 (24)				
25	δ	A′	537	539 (2)				
26	δ	A′	516	515 (0)				
27	γ	A″	411	402 (8)				
28	δ	A′	391	384 (6)				
29	γ	A″	185	170 (14)				
30	γ	A″	132[e]	158 (26)				
MAE (modes 5−10, 12−14)				24 (19)[f]	36	20	25	
MAX				53	98	33	47	

[a]All data in cm^{-1}. Harmonic frequencies at B3LYP/AN07D level, anharmonic shifts at DFTBA level. In parentheses, the absolute errors with respect to experimental frequencies. Errors of uracil have been computed with respect to gas-phase measurements. Errors of uracil+4H_2O, uracil+PCM, and uracil+4H_2O+PCM have been computed with respect to measurements in aqueous solution. Mean Absolute Errors (MAE) have been computed with reference to experimental frequencies. δ and γ are in plane and out of plane modes, respectively. [b]Biczysko et al.[82] and references therein. [c]Experimental frequencies from Raman spectra of Berthier et al.[90] [d]Experimental frequencies from IR spectra of Berthier et al.[90] [e]Not experimentally available (the value of hybrid CC/DFT calculations from Biczysko et al.[82] has been used). [f]MAE in parentheses refers to all modes.

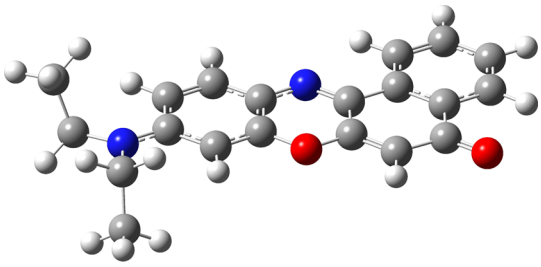

Figure 4. The most stable conformer of Nile Red.[86,87]

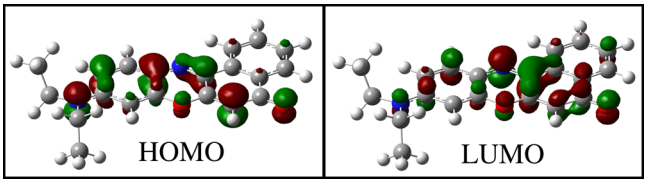

Figure 5. HOMO and LUMO molecular orbitals of Nile Red, as computed at DFTB level in this work.

4.6. Test Cases: Solvation Effects on the Electronic Energies of Nile Red and Uracil. As a concluding remark, we propose two examples of the application of the time dependent approach to the computation of the solvent effects on the vertical excitation energies.

The Nile Red molecule (shown in Figure 4) is a very interesting dye due to its peculiar electronic properties,[86,87] such as significant solvatochromic shifts on the absorption maxima and a dual fluorescence in the emission spectrum. In Table 13, the vertical excitation energies of the HOMO−LUMO transition of the Nile Red in different solvents computed with the TD-DFTB/PCM scheme are reported and compared with other experimental and computational results, available in the literature. The solvatochromic shifts at the TD-DFTB/PCM level are in quantitative agreement with the experimental energies, the maximum error being about 0.1 eV in heptane and acetonitrile solvents, and just 0.01 eV in benzene. These errors are comparable with the errors of the DFT calculations, and much lower than the errors of the CIS-HF/PCM method, for which, despite the large basis set employed, discrepancies larger than 1.5 eV are found for benzene and acetonitrile solvents. The orbitals involved in the

dx.doi.org/10.1021/ct301050x | J. Chem. Theory Comput. 2013, 9, 2052−2071

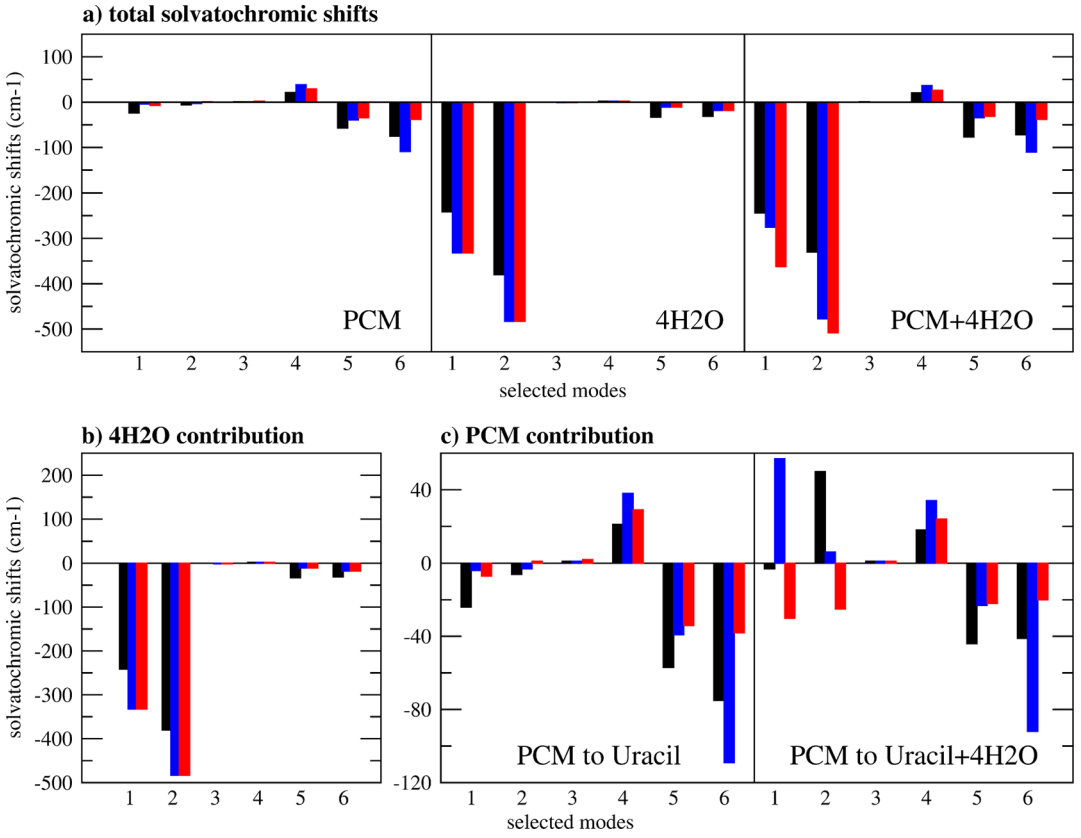

Figure 6. Solvatochromic shifts in cm^{-1} of the harmonic frequencies of uracil in aqueous solution, modeled using different computational approaches. Mode labels on each *x* axis have been defined in Table 10. Black bars refer to DFT computations, blue bars to DFTBA(0.8/0.9), and red bars to DFTBA(1.1), see Table 10 for the numerical values of the harmonic frequencies. (a) Solvatochromic shifts computed with respect to the harmonic frequencies of uracil in the gas phase. (b) Contribution to the total solvatochromic shift due to the inclusion of four explicit water molecules (i.e., the difference between the harmonic frequencies of uracil+4H_2O and uracil in the gas phase). (c) Contribution to the total solvatochromic shift due to the PCM (i.e., the difference between the harmonic frequencies of uracil+PCM and uracil+4H_2O+PCM with respect to the harmonic frequencies of uracil and uracil+4H_2O, respectively).

transition of Nile Red in the gas phase are shown in Figure 5, and they suggest that the electronic transition leads to an intramolecular charge transfer, in agreement with other results obtained at the DFT level (see Rappon et al.[86] and references therein).

The calculation of the vertical excitation energies of uracil in aqueous solution is more challenging, since both explicit water molecules and bulk effects need to be considered in order to correctly compute the energies of the $n \rightarrow \pi^*$ and $\pi \rightarrow \pi^*$ transitions. In Figure 3, the first shell of solvation of uracil, including four water molecules, has been shown. As reported by Improta and Barone,[24] the solvatochromic shifts of such transitions are significantly affected by either specific interactions between the water molecules and the lone pairs of the oxygen atoms of uracil, and by the electrostatic interaction between the bulk and the dipole moments of the ground and excited states. For these reasons, gas phase calculations usually lead to an incorrect ordering of the excited states with respect to the experiments. Thus, this system is an interesting test case in order to discuss the performances of our TD-DFTB/PCM approach. We first optimized the geometries of uracil in the gas phase and with different solvation models (uracil+PCM, uracil +4H_2O, and uracil+4H_2O+PCM), using the DFTBA method, and default cavities for PCM calculations, then we computed the transition energies at the DFTBA(1.1) level. Also, single point calculations using the reduced cavity scaling factor (α = 0.8/0.9), pure DFT methods (PBE/STO-3G and PBE-AVTZ), and hybrid DFT methods (B3LYP/AVTZ, PBE0/AVTZ) have been performed on the same geometries, in order to compare the DFTBA results with more accurate methods. In Table 12, the transition energies of the $n \rightarrow \pi^*$ and $\pi \rightarrow \pi^*$ transitions are reported, along with accurate results obtained at the PBE0 level with extended basis sets,[24] for which discrepancies lower than 0.1 eV have been found with respect to experimental results (see the original work for details). When hybrid functionals are used in conjunction with the most accurate solvent model (uracil+4H_2O+PCM), the inversion of the first and second excited states is observed, in agreement with the results reported in the literature. Such an inversion is due to the strong blue-shift of the $n \rightarrow \pi^*$ transition (about 0.5 eV), while the energy of the $\pi \rightarrow \pi^*$ is slightly affected by the solvent (red shift of less than 0.2 eV), since the variation of the dipole moment is very small. Using pure DFT functionals (see the PBE/AVTZ results), we note similar effects on the transition energies, with a sensible blue shift of the $n \rightarrow \pi^*$ transition (0.45 eV), and a very small variation of the energy associated with the $\pi \rightarrow \pi^*$. By the way, although the solvatochromic shifts are in quantitative agreement with the hybrid functionals, the total transition energies are quite different, due to a bias error affecting the gas phase energies. For this reason, we do not observe any inversion of the stability of the excited states in water. In DFTBA calculations, from a qualitative point of view,

Table 12. Vertical Energies of Uracil in Aqueous Solution[a]

	gas phase	uracil +PCM	uracil +4H_2O	uracil +4H_2O +PCM
		$n\rightarrow\pi^*$		
DFTBA(1.1)	3.64 (0.00)	3.90 (0.00)	3.79 (0.00)	3.97 (0.00)
DFTBA(0.8/0.9)	3.64 (0.00)	4.18 (0.00)	3.79 (0.00)	4.18 (0.00)
PBE/STO-3G	3.30 (0.00)	3.23 (0.00)	3.32 (0.00)	3.40 (0.00)
PBE/AVTZ	3.85 (0.00)	4.10 (0.00)	4.11 (0.00)	4.30 (0.00)
B3LYP/AVTZ	4.53 (0.00)	4.79 (0.00)	4.95 (0.00)	5.00 (0.00)
PBE0/AVTZ	4.65 (0.00)	4.90 (0.00)	4.94 (0.00)	5.11 (0.00)
PBE0[b]	4.80 (0.00)	5.09 (0.00)	4.97 (0.00)	5.28 (0.00)
		$\pi\rightarrow\pi^*$		
DFTBA(1.1)	4.73 (0.03)	4.76 (0.07)	4.66 (0.03)	4.74 (0.08)
DFTBA(0.8/0.9)	4.73 (0.03)	4.82 (0.10)	4.66 (0.03)	4.78 (0.10)
PBE/STO-3G	4.90 (0.01)	4.81 (0.02)	4.43 (0.00)	4.58 (0.01)
PBE/AVTZ	4.60 (0.05)	4.56 (0.09)	4.52 (0.02)	4.60 (0.10)
B3LYP/AVTZ	5.01 (0.11)	4.95 (0.16)	5.01 (0.07)	4.93 (0.17)
PBE0/AVTZ	5.13 (0.13)	5.05 (0.18)	5.06 (0.14)	5.03 (0.19)
PBE0[b]	5.26 (0.14)	5.17 (0.19)	5.26 (0.14)	5.16 (0.20)

[a]All geometries optimized at DFTBA level, with α = 1.1 when PCM is applied. C-PCM model has been used for consistency with reference DFT caculations. The difference between C-PCM and IEF-PCM vertical energies are on the third decimal digits. Oscillator strenghts have been reported in parentheses. Assignment of transitions have been checked by comparison with the oscillator strenghts reported in the literature and by visual inspection of molecular orbitals. [b]PBE0/6-311+G(2d,2p) energies on PBE0/6-31+G(d,p) geometries, taken from Improta et al.[24]

both the cavity scaling factors lead to similar results, showing the blue-shift of the $n\rightarrow\pi^*$ transition and very small variations of the energy of the $\pi \rightarrow \pi^*$ transition. From a quantitative point of view, the default cavity leads to an underestimation of the solvatochromic shift of the $n \rightarrow \pi^*$ (0.33 eV), while the smaller cavity reproduces it in quantitative agreement with reference results (0.54 eV). This is due to the enhanced solute−solvent electrostatic interaction and is in line with the discussion about the energetics of solvation in section 4.1. In analogy with the PBE/AVTZ calculations, the correct ordering of the excited states is not observed because of the underestimation of the energy of the $n \rightarrow \pi^*$ transition in the gas phase, while the solvation effects are very well computed employing the uracil+4H_2O+PCM solvation model. Finally, it is worth it to note that also the oscillator strenghts computed by the DFTBA(0.8/0.9) method are very similar to the ones computed at the PBE/AVTZ level. So, as a final remark we can summarize that in the proposed test cases the TD-DFTB/PCM method shows an accuracy higher than the CIS-HF/PCM and the TD-PBE/STO-3G approaches, resembling the results of a pure DFT method employing a large basis set.

5. CONCLUSIONS

In this paper, we have reported the essential details of a new fully coherent and numerically efficient implementation of DFT/PCM and TD-DFTB/PCM models including energies for ground and excited electronic states together with analytical gradients and Hessians for ground states. From the one side, numerical differentiation of analytical Hessians gives access to anharmonic computations in solution by the latest effective and stable generalizations of second order vibrational perturbation theory. From the other side, availability of TD-DFT/PCM allows the study of photophysical and photochemical processes involving large species in solution. Since the accuracy of DFTB/PCM and TD-DFTB/PCM results rivals that of the DFT model from which they were derived, this leaves room for further improvement by parametrizing the method with respect to more accurate references. Already at the present stage, coupling our approach with a more refined QM model for a reduced part of the system and/or lower-order Taylor series expansion of the potential energy surface (e.g., harmonic vs anharmonic approximation) provides results of high accuracy. Although further development is surely in order along those and related routes (e.g., TD-DFTB/PCM analytical gradients), we think that our implementation already represents a new useful tool for the computational spectroscopy studies of large systems in condensed phases.

APPENDIX: ESTIMATION OF THE INTEGRALS

It is well-known that linear combinations of Gaussian-type functions can reproduce very well the trend of the atomic orbitals χ_μ. As a consequence, the integrals on both sides of eq 34 can be evaluated in terms of Gaussian distributions for the electronic densities χ_μ and χ_ν. The integral on the right-hand side of eq 34 is then a two-center integral involving a Gaussian function with exponent α located on atom A and a Gaussian function with exponent β located on atom B (neglecting the

Table 13. Vertical Excitation Energies (eV) Corresponding to the HOMO−LUMO Transition of Nile Red (See Figures 4 and 5), in Different Solvents

		solvent effect on the vertical excitation energies					
solvent	dielectric constant	TD-DFTBA	TD-B3LYP[a] 6-31+G(d)	CIS-HF[a] 6-31+G(d)	TD-B3LYP[b] 6-311G(d,p)	TD-PBE0[b] 6-311G(d,p)	exptl.
gas phase		2.47	2.68	4.11	2.74	2.83	
heptane	1.9113	2.32			2.58	2.65	2.43[b]
benzene	2.2706	2.30	2.47	3.86			2.31[a]
acetonitrile	35.688	2.25	2.40	3.78			2.14[a]

[a]Rappon et al.[86] and references therein. [b]Mennucci al.[87] and references therein.

normalization coefficients). This integral has an analytical known solution

$$\int d\vec{r}'\, e^{-\alpha|\vec{r}'-\vec{R}_A|^2}\vec{r}'\, e^{-\beta|\vec{r}'-\vec{R}_B|^2} = \left(\frac{\pi}{\alpha+\beta}\right)^{3/2} \exp\left(-\frac{\alpha\beta}{\alpha+\beta}\left|\vec{R}_A-\vec{R}_B\right|^2\right)\left(\frac{\alpha\vec{R}_A+\beta\vec{R}_B}{\alpha+\beta}\right) \quad (44)$$

where α and β in principle are different. On the right-hand side of eq 34, we have the overlap integral, which can be analogously estimated

$$\int d\vec{r}'\, e^{-\alpha|\vec{r}'-\vec{R}_A|^2}\, e^{-\beta|\vec{r}'-\vec{R}_B|^2} = \left(\frac{\pi}{\alpha+\beta}\right)^{3/2} \exp\left(-\frac{\alpha\beta}{\alpha+\beta}\left|\vec{R}_A-\vec{R}_B\right|^2\right) \quad (45)$$

Substituting these two expressions in eq 34, we find that the computation of the dipole moment using the density of eq 18 rather than eq 3 is equivalent to using fixed, unitary values for the exponents of the Gaussian functions.

$$\left(\frac{\alpha\vec{R}_A+\beta\vec{R}_B}{\alpha+\beta}\right) \simeq \left(\frac{\vec{R}_A+\vec{R}_B}{2}\right) \quad (46)$$

We can also estimate the integrals of the electrostatic potential using Gaussian distributions

$$\vec{R}_P = \frac{\alpha\vec{R}_A+\beta\vec{R}_B}{\alpha+\beta}$$

$$\int d\vec{r}'\, \frac{e^{-\alpha|\vec{r}'-\vec{R}_A|^2} e^{-\beta|\vec{r}'-\vec{R}_B|^2}}{|\vec{r}-\vec{r}'|} = \left(\frac{\pi}{\alpha+\beta}\right)^{3/2} \exp\left(-\frac{\alpha\beta}{\alpha+\beta}|\vec{R}_A-\vec{R}_B|^2\right) \frac{\mathrm{erf}\left(\sqrt{(\alpha+\beta)|\vec{r}-\vec{R}_P|^2}\right)}{|\vec{r}-\vec{R}_P|^2} \quad (47)$$

Equation 23 then reduces to

$$\frac{\mathrm{erf}\left(\sqrt{(\alpha+\beta)|\vec{r}-\vec{R}_P|^2}\right)}{|\vec{r}-\vec{R}_P|^2} \simeq \frac{1}{2}\left(\frac{1}{|\vec{r}-\vec{R}_A|}+\frac{1}{|\vec{r}-\vec{R}_B|}\right) \quad (48)$$

which is formally exact when the point $\vec{r}$ at which the potential is evaluated is far from the location of the sources.

AUTHOR INFORMATION

Corresponding Author

*E-mail: ivan.carnimeo@sns.it.

Notes

The authors declare no competing financial interest.

REFERENCES

(1) Pedone, A.; Biczysko, M.; Barone, V. *ChemPhysChem* **2010**, *11*, 1812.

(2) Murugan, N.; Kongsted, J.; Rinkevicius, Z.; Aidas, K.; Agren, H. *J. Phys. Chem. B* **2010**, *114*, 13349.

(3) Pedone, A.; Prampolini, G.; Monti, S.; Barone, V. *Phys. Chem. Chem. Phys.* **2011**, *13*, 16689.

(4) *Computational Strategies for Spectroscopy, from Small Molecules to Nano Systems.*; Barone, V., Ed.; John Wiley & Sons, Inc: Hoboken, NJ, 2011.

(5) *Calculation of the Electronic Spectra of Large Molecules, Reviews in Computational Chemistry*; Grimme, S., Ed.; John Wiley & Sons, Inc.: New York, 2004.

(6) Barone, V.; Baiardi, A.; Biczysko, M.; Bloino, J.; Cappelliad, C.; Lipparini, F. *Phys. Chem. Chem. Phys.* **2012**, *14*, 12404.

(7) Biczysko, M.; Bloino, J.; Brancato, G.; Cacelli, I.; Cappelli, C.; Ferretti, A.; Lami, A.; Monti, S.; Pedone, A.; Prampolini, G.; Puzzarini, C.; Santoro, F.; Trani, F.; Villani, G. *Theor. Chim. Acc.* **2012**, *131*, 1201.

(8) Lipparini, F.; Barone, V. *J. Chem. Theory Comput.* **2011**, *7*, 3711.

(9) Lipparini, F.; Cappelli, C.; Barone, V. *J. Chem. Theory Comput.* **2012**, *8*, 4153.

(10) Curutchet, C.; Munoz-Losa, A.; Monti, S.; Kongsted, J.; Scholes, G.; Mennucci, B. *J. Chem. Theory Comput.* **2009**, *5*, 1838.

(11) Steindal, A.; Ruud, K.; Frediani, L.; Aidas, K.; Kongsted, J. *J. Phys. Chem. B* **2011**, *115*, 3027.

(12) Elstner, M.; Porezag, D.; Jungnickel, G.; Elsner, J.; Haugk, M.; Frauenheim, T.; Suhai, S.; Seifert, G. *Phys. Rev. B* **1998**, *58*, 7260.

(13) Zheng, G.; Lundberg, M.; Jakowski, J.; Vreven, T.; Frisch, M. J.; Morokuma, K. *Int. J. Quantum Chem.* **2009**, *109*, 1841.

(14) Harris, J. *Phys. Rev. B* **1985**, *31*, 1770.

(15) Matthew, W.; Foulkes, C.; Haydock, R. *Phys. Rev. B* **1989**, *39*, 12520.

(16) Koskinen, P.; Makinen, V. *Comp. Mater. Sci.* **2009**, *47*, 237.

(17) Witek, H.; Irle, S.; Morokuma, K. *J. Chem. Phys.* **2004**, *121*, 5163.

(18) Witek, H.; Morokuma, K. *J. Comput. Chem.* **2004**, *25*, 1858.

(19) Sattelmeyer, K. W.; Tirado-Rives, J.; Jorgensen, W. *J. Phys. Chem. A* **2006**, *110*, 13551.

(20) Trani, F.; Barone, V. *J. Chem. Theory Comput.* **2011**, *7*, 713.

(21) Niehaus, T. A.; Suhai, S.; Sala, F. D.; Lugli, P.; Elstner, M.; Seifert, G.; Frauenheim, T. *Phys. Rev. B* **2001**, *63*, 085108.

(22) Trani, F.; Scalmani, G.; Zheng, G. S.; Carnimeo, I.; Frisch, M. J.; Barone, V. *J. Chem. Theory Comput.* **2011**, *7*, 3304.

(23) Jamorski, C.; Casida, M.; Salahub, D. *J. Chem. Phys.* **1996**, *104*, 5134.

(24) Improta, R.; Barone, V. *J. Am. Chem. Soc.* **2004**, *126*, 14320.

(25) Barone, V.; Cossi, M. *J. Phys. Chem. A* **1998**, *102*, 1995.

(26) Cossi, M.; Rega, N.; Scalmani, G.; Barone, V. *J. Comput. Chem.* **2003**, *24*, 669.

(27) Cossi, M.; Barone, V.; Cammi, R.; Tomasi, J. *J. Chem. Phys. Lett.* **1996**, *255*, 327.

(28) Cances, E.; Mennucci, B.; Tomasi, J. *J. Chem. Phys.* **1997**, *107*, 3032.

(29) Cances, E.; Mennucci, B. *J. Math. Chem.* **1998**, *23*, 309.

(30) Mennucci, B.; Cances, E.; Tomasi, J. *J. Phys. Chem. B* **1997**, *101*, 10506.

(31) Cappelli, C.; Corni, S.; Cammi, R.; Mennucci, B.; Tomasi, J. *J. Chem. Phys.* **2000**, *113*, 11270.

(32) Cappelli, C.; Lipparini, F.; Bloino, J.; Barone, V. *J. Chem. Phys.* **2011**, *135*, 104505.

(33) Mennucci, B.; Cammi, R.; Tomasi, J. *J. Chem. Phys.* **1998**, *109*, 2798.

(34) Lipparini, F.; Cappelli, C.; Scalmani, G.; Mitri, N. D.; Barone, V. *J. Chem. Theory Comput.* **2012**, *8*, 4270.

(35) Lipparini, F.; Scalmani, S.; Mennucci, B.; Cances, E.; Caricato, M.; Frisch, M. *J. Chem. Phys.* **2010**, *133*, 014106.

(36) Lipparini, F.; Scalmani, S.; Mennucci, B.; Frisch, M. *J. Chem. Theory Comput.* **2011**, *7*, 610.

(37) Malolepsza, E.; Witek, H.; Morokuma, K. *Chem. Phys. Lett.* **2005**, *412*, 237.

(38) Gaus, M.; Chou, C.; Witek, H.; Elstner, M. *J. Phys. Chem. A* **2009**, *113*, 11866.

(39) Bodrog, Z.; Aradi, B.; Frauenheim, T. *J. Chem. Theory Comput.* **2011**, *7*, 2654.

(40) Kazachkin, D.; Nishimura, Y.; Witek, H.; Irle, S.; Borguet, E. *J. Am. Chem. Soc.* **2011**, *133*, 8191.

(41) Li, W.; Irle, S.; Witek, H. *ACS Nano* **2010**, *4*, 4475.
(42) Malolepsza, E.; Lee, Y.; Witek, H.; Irle, S.; Lin, C.; Hsieh, H. *Int. J. Quantum Chem.* **2009**, *109*, 1999.
(43) Kaminski, S.; Gaus, M.; Phatak, P.; von Stetten, D.; Elstner, M.; Mroginski, M. *J. Chem. Theory Comput.* **2010**, *6*, 1240.
(44) Simon, A.; Rapacioli, M.; Mascetti, J.; Spiegelman, F. *Phys. Chem. Chem. Phys.* **2012**, *14*, 6771.
(45) Elstner, M.; Hobza, P.; Frauenheim, T.; Suhai, S.; Kaxiras, E. *J. Chem. Phys.* **2001**, *114*, 5149.
(46) Rapacioli, M.; Spiegelman, F.; Talbi, D.; Minerva, T.; Goursot, A.; Heine, T.; Seifert, G. *J. Chem. Phys.* **2009**, *130*, 244304.
(47) Li, J.; Zhu, T.; Cramer, C.; Truhlar, D. *J. Phys. Chem. A* **1998**, *102*, 1820.
(48) Kalinowski, J.; Lesnyg, B.; Thompson, J.; Cramer, C.; Truhlar, D. *J. Phys. Chem. A* **2004**, *108*, 2545.
(49) Barone, V. *J. Chem. Phys.* **2004**, *120*, 3059.
(50) Barone, V. *J. Chem. Phys.* **2005**, *122*, 014108.
(51) Bloino, J.; Biczysko, M.; Barone, V. *J. Chem. Theory Comput.* **2012**, *8*, 1015.
(52) Lu, Z.; Liu, H.; Elstner, M.; Yang, W. *Reviews of Modern Quantum Chemistry: A Celebration of the Contribution of Robert G. Parr*; World Scientific Pub. Co., Inc.: River Edge, NJ, 2002; p 1606.
(53) Hou, G.; Zhu, X.; Cui, Q. *J. Chem. Theory Comput.* **2010**, *6*, 2303.
(54) Xie, L.; Liu, H. *J. Comput. Chem.* **2002**, *23*, 1404.
(55) Cossi, M.; Scalmani, G.; Rega, N.; Barone, V. *J. Chem. Phys.* **2002**, *117*, 43.
(56) Scalmani, G.; Frisch, M. J. *J. Chem. Phys.* **2010**, *132*, 114110.
(57) Barone, V.; Cossi, M.; Tomasi, J. *J. Chem. Phys.* **1997**, *107*, 3210.
(58) Cammi, R.; Tomasi, J. *J. Chem. Phys.* **1994**, *100*, 7495.
(59) Cammi, R.; Tomasi, J. *J. Chem. Phys.* **1994**, *101*, 3888.
(60) Cossi, M.; Barone, V. *J. Chem. Phys.* **2001**, *115*, 4708.
(61) Stewart, J. J. P. *J. Mol. Model.* **2007**, *13*, 1173.
(62) Dewar, M.; Zoebisch, E.; Healy, E.; Stewart, J. *J. Am. Chem. Soc.* **1985**, *107*, 3902.
(63) Becke, A. D. *J. Chem. Phys.* **1993**, *98*, 5648.
(64) Neese, F.; Schwabe, T.; Grimme, S. *J. Chem. Phys.* **2007**, *126*, 124115.
(65) Kozuch, S.; Gruzman, D.; Martin, J. *J. Phys. Chem. C* **2010**, *114*, 20801.
(66) Biczysko, M.; Panek, P.; Scalmani, G.; Bloino, J.; Barone, V. *J. Chem. Theory Comput.* **2010**, *6*, 2115.
(67) Biczysko, M.; Bloino, J.; Carnimeo, I.; Panek, P.; Barone, V. *J. Mol. Struct.* **2012**, *1009*, 74.
(68) Carbonniere, P.; Barone, V. *Chem. Phys. Lett.* **2004**, *399*, 226.
(69) Perdew, J. P.; Burke, K.; Ernzerhof, M. *Phys. Rev. Lett.* **1996**, *77*, 3865.
(70) Barone, V.; Cossi, M.; Tomasi, J. *J. Chem. Phys.* **1997**, *107*, 3210.
(71) Frisch, J.; Trucks, G. W.; Schlegel, H. B.; Scuseria, G. E.; Robb, M. A.; Cheeseman, J. R.; Scalmani, G.; Barone, V.; Mennucci, B.; Petersson, G. A.; Nakatsuji, H.; Caricato, M.; Li, X.; Hratchian, H. P.; Izmaylov, A. F.; Bloino, J.; Zheng, G.; Sonnenberg, J. L.; Hada, M.; Ehara, M.; Toyota, K.; Fukuda, R.; Hasegawa, J.; Ishida, M.; Nakajima, T.; Honda, Y.; Kitao, O.; Nakai, H.; Vreven, T.; Montgomery, J. A., Jr.; Peralta, J. E.; Ogliaro, F.; Bearpark, M.; Heyd, J. J.; Brothers, E.; Kudin, K. N.; Staroverov, V. N.; Kobayashi, R.; Normand, J.; Raghavachari, K.; Rendell, A.; Burant, J. C.; Iyengar, S. S.; Tomasi, J.; Cossi, M.; Rega, N.; Millam, J. M.; Klene,M.; Knox, J. E.; Cross, J. B.; Bakken, V.; Adamo, C.; Jaramillo, J.; Gomperts, R.; Stratmann, R. E.; Yazyev, O.; Austin, A. J.; Cammi, R.; Pomelli, C.; Ochterski, J. W.; Martin, R. L.; Morokuma, K.; Zakrzewski, V. G.; Voth, G. A.; Salvador, P.; Dannenberg, J. J.; Dapprich, S.; Daniels, A. D.; Farkas, Ã.; Foresman, J. B.; Ortiz, J. V.; Cioslowski, J.; Fox, D. J. *Gaussian GDV, Revision H.21*; Gaussian Inc.: Wallingford, CT, 2009.
(72) Rapacioli, M.; Simon, A.; Dontot, L.; Spiegelman, F. *Phys. Status Solidi B* **2012**, *249*, 245.
(73) Giese, T.; York, D. *Theor. Chim. Acc.* **2012**, *131*, 1145.
(74) Giese, T.; York, D. *J. Chem. Phys.* **2011**, *134*, 194103.
(75) Gaus, M.; Cui, Q.; Elstner, M. *J. Chem. Theory Comput.* **2010**, *7*, 931.
(76) Gaus, M.; Goez, A.; Elstner, M. *J. Chem. Theory Comput.* **2013**, *9*, 338.
(77) Kaminski, S.; Gaus, M.; Elstner, M. *J. Phys. Chem. A* **2012**, *116*, 11927.
(78) Kubar, T.; Elstner, M. *J. Phys. Chem. B* **2010**, *114*, 11221.
(79) Hourahine, B.; Sanna, S.; Aradi, B.; Niehaus, T.; Frauenheim, T. *J. Phys. Chem. A* **2007**, *111*, 5671.
(80) Lundberg, M.; Nishimoto, Y.; Irle, S. *Int. J. Quantum Chem.* **2011**, *112*, 1701.
(81) Puzzarini, C.; Biczysko, M.; Barone, V. *J. Chem. Theory Comput.* **2010**, *6*, 828.
(82) Puzzarini, C.; Biczysko, M.; Barone, V. *J. Chem. Theory Comput.* **2011**, *7*, 3702.
(83) Begue, D.; Carbonniere, P.; Pouchan, C. *J. Phys. Chem. A* **2005**, *109*, 4611.
(84) Barone, V.; Biczysko, M.; Bloino, J.; Borkowska-Panek, M.; Carnimeo, I.; Panek, P. *Int. J. Quantum Chem.* **2012**, *112*, 2185.
(85) Carnimeo, I.; Biczysko, M.; Bloino, J.; Barone, V. *Phys. Chem. Chem. Phys.* **2011**, *13*, 16713.
(86) Tuck, P. O.; Mawhinney, R. C.; Rappon, M. *Phys. Chem. Chem. Phys.* **2009**, *11*, 4471.
(87) Guido, C.; Mennucci, B.; Jacqueminc, D.; Adamo, C. *Phys. Chem. Chem. Phys.* **2010**, *12*, 8016.
(88) Wiberg, K. B.; Thiel, Y.; Goodman, L.; Leszczynski, J. *J. Phys. Chem.* **1995**, *99*, 13850.
(89) Olbert-Majkut, A.; Ahokas, J.; Lundell, J.; Pettersson, M. *J. Raman Spectrosc.* **2011**, *42*, 1670.
(90) Aamouche, A.; Ghomi, M.; Coulombeau, C.; Jobic, H.; Grajcar, L.; Baron, M.; Baumruk, V.; Turpin, P.; Henriet, C.; Berthier, G. *J. Phys. Chem.* **1996**, *100*, 5224.